

THE EARLY DETECTION AND FOLLOW-UP OF THE HIGHLY OBSCURED TYPE II SUPERNOVA
2016IJA/DLT16AM*

L. TARTAGLIA,^{1,2} D. J. SAND,¹ S. VALENTI,² S. WYATT,¹ J. P. ANDERSON,³ I. ARCAVI,^{4,5,6} C. ASHALL,⁷
M. T. BOTTICELLA,⁸ R. CARTIER,⁹ T.-W. CHEN,¹⁰ A. CIKOTA,¹¹ D. COULTER,¹² M. DELLA VALLE,⁸ R. J. FOLEY,¹²
A. GAL-YAM,¹³ L. GALBANY,¹⁴ C. GALL,¹⁵ J. B. HAISLIP,¹⁶ J. HARMANEN,¹⁷ G. HOSSEINZADEH,^{4,5} D. A. HOWELL,^{4,5}
E. Y. HSIAO,¹⁸ C. INSERRA,⁹ S. W. JHA,¹⁹ E. KANKARE,²⁰ C. D. KILPATRICK,¹² V. V. KROUPRIANOV,¹⁶
H. KUNCARAYAKTI,^{21,17} T. J. MACCARONE,²² K. MAGUIRE,²⁰ S. MATTILA,¹⁷ P. A. MAZZALI,^{7,23} C. MCCULLY,^{4,5}
A. MELANDRI,²⁴ N. MORRELL,²⁵ M. M. PHILLIPS,²⁵ G. PIGNATA,^{26,27} A. L. PIRO,²⁸ S. PRENTICE,⁷ D. E. REICHAUT,¹⁶
C. ROJAS-BRAVO,¹² S. J. SMARTT,²⁰ K. W. SMITH,²⁰ J. SOLLERMAN,²⁹ M. D. STRITZINGER,³⁰ M. SULLIVAN,⁹ F. TADDIA,²⁹
AND D. R. YOUNG²⁰

¹Department of Astronomy and Steward Observatory, University of Arizona, 933 N Cherry Ave, Tucson, AZ 85719, USA

²Department of Physics, University of California, 1 Shields Ave, Davis, CA 95616, USA;

³European Southern Observatory, Alonso de Córdova 3107, Casilla 19, Santiago, Chile

⁴Department of Physics, University of California, Santa Barbara, CA ,93106-9530, USA

⁵Las Cumbres Observatory, 6740 Cortona Dr., Suite 102, Goleta, CA 93117, USA

⁶Einstein Fellow

⁷Astrophysics Research Institute, Liverpool John Moores University, IC2, Liverpool Science Park, 146 Brownlow Hill, Liverpool L3 5RF, UK

⁸INAF - Osservatorio Astronomico di Capodimonte, Salita Moiariello 16, Napoli, 80131 Italy

⁹School of Physics and Astronomy, University of Southampton, Southampton, SO17 1BJ, UK

¹⁰Max-Planck-Institut für Extraterrestrische Physik, Giessenbachstraße 1, 85748, Garching, Germany

¹¹European Southern Observatory, Karl-Schwarzschild-Str. 2, 85748 Garching b. München, Germany

¹²Department of Astronomy and Astrophysics, University of California, Santa Cruz, CA 95064, USA

¹³Benoziyo Center for Astrophysics, Faculty of Physics, Weizmann Institute of Science, Rehovot 76100, Israel

¹⁴PITT PACC, Department of Physics and Astronomy, University of Pittsburgh, Pittsburgh, PA 15260, USA

¹⁵Dark Cosmology Centre, Niels Bohr Institute, University of Copenhagen, Juliane Maries Vej, 30, 2100 Copenhagen

¹⁶Department of Physics and Astronomy, University of North Carolina at Chapel Hill, Chapel Hill, NC 27599

¹⁷Tuorla Observatory, Department of Physics and Astronomy, University of Turku, Väisäläntie 20, FI-21500 Piikkiö, Finland

¹⁸Department of Physics, Florida State University, Keen Building 616, Tallahassee, FL 3206-4350

¹⁹Department of Physics and Astronomy, Rutgers, the State University of New Jersey, 136 Frelinghuysen Road, Piscataway, NJ 08854, USA

²⁰Astrophysics Research Centre, School of Mathematics and Physics, Queen's University Belfast, Belfast BT7 1NN, UK

²¹Finnish Centre for Astronomy with ESO (FINCA), University of Turku, Väisäläntie 20, 21500 Piikkiö, Finland

²²Department of Physics, Texas Tech University, Box 41051, Lubbock, TX 79409-1051, USA

²³Max-Planck-Institut für Astrophysik, Karl-Schwarzschild-Str. 1, 85748 Garching bei München, Germany

²⁴INAF - Osservatorio Astronomico di Brera, via E. Bianchi 36, I-23807 Merate (LC), Italy

²⁵Carnegie Observatories, Las Campanas Observatory, Casilla 601, La Serena, Chile

²⁶Departamento de Ciencias Físicas, Universidad Andres Bello, Avda. Republica 252, Santiago, Chile

²⁷Millennium Institute of Astrophysics (MAS), Nuncio Monseor Stero Sanz 100, Providencia, Santiago, Chile

²⁸The Observatories of the Carnegie Institution for Science, 813 Santa Barbara St., Pasadena, CA 91101, USA

²⁹Department of Astronomy and The Oskar Klein Centre, AlbaNova University Center, Stockholm University, SE-106 91 Stockholm, Sweden

³⁰Department of Physics and Astronomy, Aarhus University, Ny Munkegade 120, DK-8000 Aarhus C, Denmark

Corresponding author: L. Tartaglia
ltartaglia@ucdavis.edu

* This paper includes data gathered with the 6.5 meter Magellan Telescopes located at Las Campanas Observatory, Chile.

(Received 2017-10-07)

Submitted to The Astrophysical Journal

ABSTRACT

We present our analysis of the Type II supernova DLT16am (SN 2016ija). The object was discovered during the ongoing $D < 40$ Mpc (DLT40) one day cadence supernova search at $r \sim 20.1$ mag in the ‘edge-on’ nearby ($D = 20.0 \pm 1.9$ Mpc) galaxy NGC 1532. The subsequent prompt and high-cadenced spectroscopic and photometric follow-up revealed a highly extinguished transient, with $E(B - V) = 1.95 \pm 0.15$ mag, consistent with a standard extinction law with $R_V = 3.1$ and a bright ($M_V = -18.49 \pm 0.65$ mag) absolute peak-magnitude. The comparison of the photometric features with those of large samples of Type II supernovae reveals a fast rise for the derived luminosity and a relatively short plateau phase, with a slope of $S_{50V} = 0.84 \pm 0.04$ mag/50 d consistent with the photometric properties typical of those of fast declining Type II supernovae. Despite the large uncertainties on the distance and the extinction in the direction of DLT16am, the measured photospheric expansion velocity and the derived absolute V -band magnitude at ~ 50 d after the explosion match the existing luminosity-velocity relation for Type II supernovae.

Keywords: galaxies: individual (NGC 1532) — supernovae: general — supernovae: individual (SN 2016ija, DLT16am)

1. INTRODUCTION

The study of cosmic explosions continues to flourish with innovative experiments exploring new regions of discovery space. Many of these programs are focusing on wide-field imaging and relatively short cadences (e.g. the Palomar Transient Factory - PTF; Law et al. 2009, the Asteroid Terrestrial-impact Last Alert System - ATLAS; Tonry 2011, the All Sky Automated Survey for SuperNovae - ASAS-SN; Shappee et al. 2014; Kochanek et al. 2017, the PANoramic Survey Telescope And Rapid Response System - Pan-STARRS1; Chambers et al. 2016, among others), resulting in hundreds of new supernovae (SNe) per year. This revolution will certainly continue in the era of the Zwicky Transient Facility (ZTF; Bellm 2014), BlackGEM¹ (Bloemen et al. 2015) and the Large Synoptic Survey Telescope (LSST; Ivezić et al. 2008). It is still the case, however, that the nearest SNe are not always caught soon after explosion, relinquishing an opportunity for detailed study of the most observable events – a recent prominent example was the type Ia SN 2014J in M82 ($D \sim 3.5$ Mpc), which was discovered ~ 8 days after explosion (Fossey et al. 2014; Goobar et al. 2015).

It is in the hours to days after explosion where clues about the SN progenitors and explosion physics are accessible, and where the fewest observational constraints are available. Early discovery and prompt multi-wavelength follow-up of nearby SNe is essential to fully characterize the physical properties of stellar explosions. Except for a few cases where deep archival *Hubble Space Telescope* (*HST*) images are available (Smartt 2009), one of the best ways to gain insight into a SN progenitor and its explosion mechanism is through the analysis of very early phase data, when the spectra still show the imprint from the outer layers of the progenitor, the explosion energy is still the dominant heat source and the circumstellar medium (CSM) has not yet been overtaken by the SN ejecta.

In Type Ia SNe, the very early light curves and spectra can help to constrain the white dwarf (WD) progenitor radius (e.g. Nugent et al. 2011; Bloom et al. 2012; Zheng et al. 2013), its ^{56}Ni distribution (from the early light curve shape; see Mazzali et al. 2014; Piro & Nakar 2014; Miller et al. 2017), to infer the presence of a normal companion star (via direct shocking of the SN Ia ejecta against the normal companion Kasen 2010; Cao et al. 2015; Marion et al. 2016; Hosseinzadeh et al. 2017) and probe SN Ia explosion mechanisms. While it is commonly accepted that SNe Ia arise from ther-

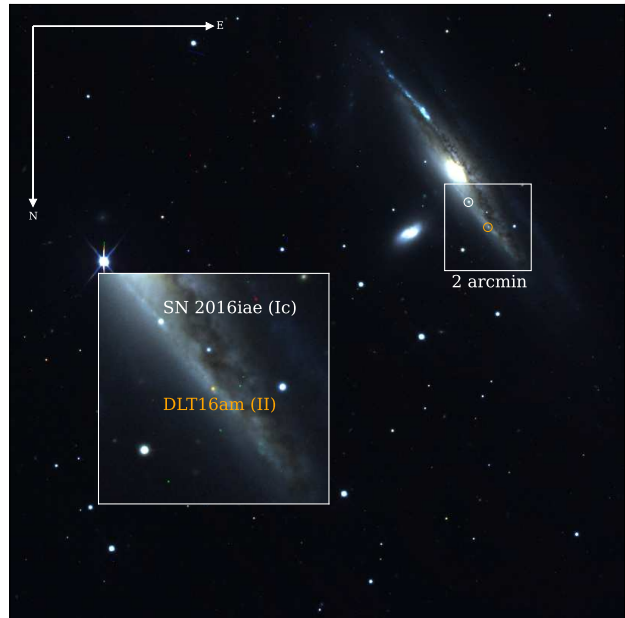


Figure 1. RGB images of the DLT16am field obtained using i , r and g -band images, respectively. The position of the Type Ic SN 2016iae is marked for reference. A zoom-in of the region of the two SNe is shown in the inset ($\sim 2'$).

monuclear explosions of carbon-oxygen WDs, it is still unclear by which mechanism(s) the WD accretes the necessary mass (single or double degenerate scenario, see, e.g., Maoz & Mannucci 2012, for a review). The detection and strength of C II (6580 Å) in early spectra may also point to viable explosion mechanisms (see, e.g., Mazzali 2001; Höflich & Stein 2002; Röpke et al. 2007; Kasen et al. 2009; Fryer et al. 2010).

Early light curves of core-collapse (CC) SN shock cooling tails can constrain the progenitor star radius and give useful information about the envelope structure (see, e.g., Rabinak & Waxman 2011; Bersten et al. 2012; Arcavi et al. 2017; Piro et al. 2017; Sapir & Waxman 2017; Barbarino et al. 2017, for selected theoretical and observational results). Alternatively, ‘flash spectroscopy’ at very early phases, can probe the physical properties of the CSM as well as the mass loss history of the progenitor star prior to its explosion (e.g. Gal-Yam et al. 2014; Khazov et al. 2016; Yaron et al. 2017). Even when archival *HST* data are available, radius estimates through the analysis of very early data can give important results, since the progenitor field might be contaminated by the presence of binary companions (e.g. Tartaglia et al. 2017i).

Motivated by the science described above, and by the need for multi-wavelength observations at very early phases, we have begun a pointed, one day cadence SN search for very young transients in the nearby

¹ <https://astro.ru.nl/blackgem/>

($D < 40$ Mpc; DLT40) Universe. Given the survey depth of $r \simeq 19$ mag and the proximity of the DLT40 galaxy sample (see Section 2), this program is also sensitive to heavily extinguished SNe. A significant number of CCSNe are likely missed by current optical surveys even in normal nearby galaxies due to dust extinction (Mattila et al. 2012; Jencson et al. 2017), which may explain the unexpectedly low CCSNe rate with respect to the cosmic star-formation rate (SFR; Horiuchi et al. 2011; Dahlen et al. 2012; Melinder et al. 2012; Cappellaro et al. 2015; Strolger et al. 2015).

In this paper we describe the highly obscured, nearby Type II SN DLT16am (SN 2016ija), the first SN discovered by the $D < 40$ Mpc (DLT40) one day cadence supernova search. DLT16am was discovered on 2016-11-21.19 UT (Tartaglia et al. 2016b) in the nearby galaxy NGC 1532 (see Figure 1). Fortuitously, the type Ic SN 2016iae (Prentice et al., in preparation) was discovered in the same galaxy ~ 2 weeks before and was being observed by a number of groups, allowing very tight constraints on the explosion time of DLT16am itself (JD = 2457712.6 \pm 1.0 d, see Section 5). The SN is located at RA=04:12:07.64, Dec=-32:51:10.57 [J2000], 42''08 E, 76''43 N offset from the center of NGC 1532. It was first suggested to be a 91T-like Type Ia SN, showing a nearly featureless and very red continuum, although subsequent early spectra revealed broad H α and calcium features on top of a red continuum, leading to a more appropriate classification as a highly reddened Type II SN². DLT16am is heavily extinguished, but we were still able to obtain a comprehensive multi-wavelength dataset, allowing a detailed comparison of its properties with standard, less extinguished Type II SNe.

This paper is organized as follows: Section 2 is a description of the DLT40 survey, while Section 3 describes the instrumental setups and the reduction tools used to carry out the follow-up campaign of DLT16am. In Section 4 we present the results of our analysis on the host galaxy, NGC 1532. Sections 5 and 6 report the main results of our photometric and spectroscopic analysis, respectively, while in Section 7 we compare the main spectroscopic and photometric features of DLT16am with those displayed by other Type II SNe. Finally, we summarize our results in Section 8.

2. THE DLT40 SURVEY

The goal of DLT40 is not to find many SNe, but ~ 10 nearby SNe per year within ~ 1 day from explosion. Fully operational since late summer 2016, we observe $\sim 300 - 600$ galaxies per night using a PROMPT

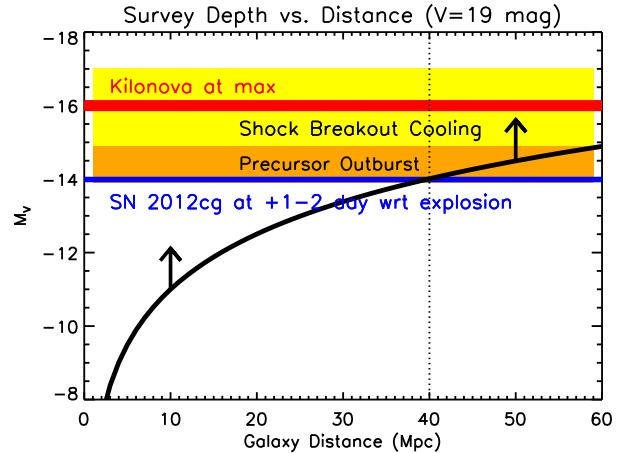


Figure 2. Absolute magnitude reached for a survey depth of $V = 19$ mag as a function of distance (black line). We highlight the magnitude range for the early SN features necessary to understand their progenitors and explosions. Also noted is the absolute magnitude of SN 2012cg $\sim 1 - 2$ days after explosion, which has possible early time light curve features which can shed light on its progenitor (Marion et al. 2016) and the V -band absolute magnitude reached by the kilonova DLT17ck (AT 2017gfo) at maximum (Valenti et al. 2017b).

0.4 m telescope (PROMPT5; Reichart et al. 2005) at the Cerro Tololo Inter-American Observatory (CTIO), achieving a typical single-epoch depth of $r \approx 19 - 20$ mag with filterless observations and a 45 s integration time.

The field of view of 10×10 arcmin² is sufficient to completely image all but the nearest galaxies. DLT40 is sensitive to most of the early observational signatures that can be used to constrain the nature of the progenitor stars, as illustrated in Figure 2.

The DLT40 galaxy sample is drawn from the nearby Gravitational Wave Galaxy Catalogue (GWGC) of White et al. (2011). From this list, we select all potential DLT40 galaxies with $M_B < -18$ mag, Milky Way (MW) extinction $A_V < 0.5$ mag and recessional velocity $v_r < 3000$ km s⁻¹, corresponding to a Hubble flow distance of $D \lesssim 40$ Mpc. Our nightly schedule is based on this list, with preference given to those fields observed in the previous three days, along with intrinsically bright ($M_B < -20$ mag) or nearby galaxies ($D < 11$ Mpc) and fields that have more than one target galaxy within the PROMPT field of view. Given the high star formation rates and stellar masses of our targets, and based on current SN rates and simulations, we expect to find ~ 20 SN yr⁻¹. Assuming some weather and instrument problems, we ultimately expect ~ 10 SN yr⁻¹ ($\sim 2 - 3$ Ia, $\sim 2 - 3$ Ib/c and $\sim 4 - 5$ Type II SNe per year) discovered within ~ 1 d of explosion. PROMPT5 DLT40 pre-reduced images are delivered

² <https://wis-tns.weizmann.ac.il/object/2016ija>

within ~ 1 minute of the data being taken, and are further processed by our pipeline, which includes quality checks, difference imaging (with HOTPANTS; Becker 2015), candidate detection and scoring (based on the difference image properties), databasing and web site generation of stamps for candidate inspection. The average lag between an observation and the visualization of the SN candidates is $\sim 3 - 4$ minutes, after which one or more team members can immediately trigger a PROMPT5 confirmation image or further observations at other facilities.

First results from the DLT40 survey were presented for the nearby Type Ia SN 2017cbv (DLT17u) in Hosseinzadeh et al. (2017), and 13 discoveries have been reported to the Astronomer’s Telegram service (Tartaglia et al. 2016a,c, 2017a,g,h,b; Sand et al. 2017a; Tartaglia et al. 2017c; Sand et al. 2017b; Tartaglia et al. 2017d,e,f; Valenti et al. 2017a), in line with our initial expectations. More DLT40 results are in preparation.

3. OBSERVATIONS AND DATA REDUCTION

Table 1. Log of the spectroscopical observations.

Date (UT)	JD	Phase (d)	Instrumental setup	Grism / Grating	Spectral range (\AA)	Exposure time (s)
20161122	2457715.144	+2	FTS+FLOYDS	235 l/mm	5000 – 9200	3600
20161123	2457716.557	+4	NOT+ALFOSC	Gr4	4000 – 9700	2400
20161124	2457717.315	+5	SALT+RSS	PG0300	3300 – 9200	2326
20161127	2457719.735	+7	ESO NTT+SOFI	GB+GR	9000 – 22000	$8 \times 270 + 8 \times 450$
20161201	2457723.753	+11	ESO NTT+EFOSC	Gr16	6000 – 10000	2700
20161213	2457736.516	+24	NOT+ALFOSC	Gr4	4000 – 9700	2400
20161219	2457742.732	+30	ESO NTT+EFOSC	Gr16	6000 – 10000	2700
20161222	2457744.517	+32	ESO VLT+X-shooter	UVB+VIS+NIR	3500 – 25000	700+600+600
20161222	2457744.881	+32	FTN+FLOYDS	235 l/mm	5000 – 9200	3600
20161224	2457746.568	+34	Gemini+GNIRS	ShortXD	8800 – 24000	3000
20161225	2457747.846	+35	FTN+FLOYDS	235 l/mm	5000 – 9200	3600
20161227	2457749.842	+37	FTN+FLOYDS	235 l/mm	5000 – 9200	3600
20170102	2457755.671	+43	Baade+FIRE	LDPrism	8800 – 20000	8×126.8
20170102	2457756.019	+43	FTS+FLOYDS	235 l/mm	5000 – 9200	3600
20170104	2457758.693	+46	ESO NTT+SOFI	GB+GR	9000 – 24000	$8 \times 270 + 8 \times 450$
20170105	2457758.945	+46	FTS+FLOYDS	235 l/mm	5000 – 9200	3600
20170107	2457760.928	+48	FTS+FLOYDS	235 l/mm	5000 – 9200	3600
20170113	2457766.815	+54	Gemini+GNIRS	ShortXD	8800 – 24000	3000
20170116	2457770.386	+58	NOT+ALFOSC	Gr4	4000 – 9700	2400
20170117	2457771.620	+59	ESO NTT+EFOSC	Gr16	6000 – 10000	2400
20170118	2457772.620	+60	ESO NTT+SOFI	GB+GR	9000 – 24000	$8 \times 270 + 8 \times 450$
20170125	2457779.635	+67	ESO NTT+EFOSC	Gr16	6000 – 10000	2400
20170204	2457789.619	+77	ESO NTT+EFOSC	Gr16	6000 – 10000	2700
20170206	2457790.591	+78	ESO NTT+SOFI	GB+GR	9000 – 24000	$6 \times 270 + 6 \times 450$
20170219	2457803.559	+91	ESO NTT+EFOSC	Gr16	6000 – 10000	2700

Table 1 continued

Table 1 (*continued*)

Date (UT)	JD	Phase (d)	Instrumental setup	Grism / Grating	Spectral range (Å)	Exposure time (s)
20170224	2457809.554	+97	ESO NTT+EFOSC	Gr16	6000 – 10000	2700
20170307	2457819.580	+107	ESO NTT+SOFI	GB	9000 – 17000	6 × 270
20170307	2457820.510	+108	ESO NTT+EFOSC	Gr16	6000 – 10000	2700

NOTE—FTN: 2 m Faulkes Telescope North, Las Cumbres Observatory node at the Haleakala Observatory, Hawaii; FTS: 2 m Faulkes Telescope South, Las Cumbres Observatory node at the Siding Spring Observatory, Australia; NOT: 2.56 m Nordic Optical Telescope, located at Roque de los Muchachos, La Palma, Spain; ESO VLT: 8.2 m Very Large Telescope, located at the ESO Cerro Paranal Observatory, Chile; ESO NTT: 3.58 m New Technology Telescope, located at the ESO La Silla Observatory, Chile; Baade: 6.5 m Magellan (Walter Baade) Telescope at the Las Campanas Observatory, Chile; Gemini: 8.19 m Gemini North Telescope at the Mauna Kea Observatories, Hawaii.

3.1. Spectra

The spectral sequence of DLT16am is shown in Figure 3, while the log of the spectroscopic observations in the optical and NIR domains is reported in Table 1. Optical spectra were mainly provided by PESSTO using the ESO 3.58 m NTT with the ESO Faint Object Spectrograph and Camera (v.2, EFOSC2 Buzzoni et al. 1984) and the Las Cumbres Observatory network of telescopes, using the 2 m Faulkes North and South telescopes with FLOYDS and reduced as in Valenti et al. (2014). Early phase spectra were also provided using the 10 m South African Large Telescope (SALT) with the Robert Stobie Spectrograph (RSS) and the 2.56 m NOT with ALFOSC. NOT spectra were reduced using FOSCGUI, while the SALT spectrum was reduced using a dedicated pipeline (PYSALT; Crawford et al. 2010a).

NIR spectra were obtained using the standard ‘ABBA’ technique and an A0V telluric standard was observed at similar airmass in order to simultaneously correct for telluric absorption and to flux calibrate the main science data, and were mainly provided by PESSTO using NTT with SOFI (all reduced as in Smartt et al. 2015). Two NIR spectra were obtained using the Gemini NIR Spectrograph (GNIRS) at Gemini North (Elias et al. 2006) in cross-dispersed mode, using the 321mm^{-1} grating and the $0''.675$ slit. This setup yields a continuous wavelength coverage from 0.8 to $2.5\ \mu\text{m}$ with a resolution of $R \sim 1000$. The data were taken with the slit along the parallactic angle, and were reduced with the XDGNIRS PyRAF-based pipeline provided by Gemini Observatory. Flux calibration and telluric correction were performed following the methodology of Vacca et al. (2003). A NIR spectrum was also obtained using the 6.5 m Magellan Baade Telescope with the Folded-port InfraRed Echelle (FIRE). The spectrum was taken in the long slit prism mode, $0''.6$ slit width, and was a combination of 8 exposures of 126.8 s each. The reduction was done us-

ing the standard ‘firehose’ IDL package (Simcoe et al. 2013).

Multi-wavelength (300 – 2500 nm) intermediate resolution spectra were obtained using the ESO *Very Large Telescope* (VLT) with X-shooter (Vernet et al. 2011), mounted at the Cassegrain focus of the 8 m VLT UT2 telescope. UVB, VIS and NIR arm data (covering the 300–559.5, 559.5–1024 and 1024–2480 nm wavelength ranges respectively) were reduced using the X-shooter dedicated pipeline through the ESOREFLEX environment (Freudling et al. 2013).

Optical and NIR spectra will be released through the Weizmann Interactive Supernova data REpository (WISEREP³; Yaron & Gal-Yam 2012).

3.2. Light curves

Photometric data are shown in Figure 4 and reported in Tables 2, 3 and 4, including publicly available early time photometry (Smith et al. 2016; Chen et al. 2016).

The *griz* data were mainly provided by the Las Cumbres Observatory (Brown et al. 2013). Additional *griz* data were obtained using the MPG/ESO 2.2 m telescope at the La Silla Observatory with the Gamma-ray Burst Optical/Near-infrared Detector (GROND; Greiner et al. 2008), which also provided early-phase photometric data at near infrared (NIR) wavelengths, the 2 m Liverpool Telescope (LT) with the optical imaging component of the Infrared-Optical camera (IO:O), the 2.56 m Nordic Optical Telescope (NOT) with the Andalucia Faint Object Spectrograph and Camera (ALFOSC) and Las Campanas Observatory 1 m Swope Telescope with an E2V camera (Bowen & Vaughan 1973). Pre-reduction steps (including bias, flat-field corrections, image stacking and astrometry calibration) for

³ <https://wiserep.weizmann.ac.il/>

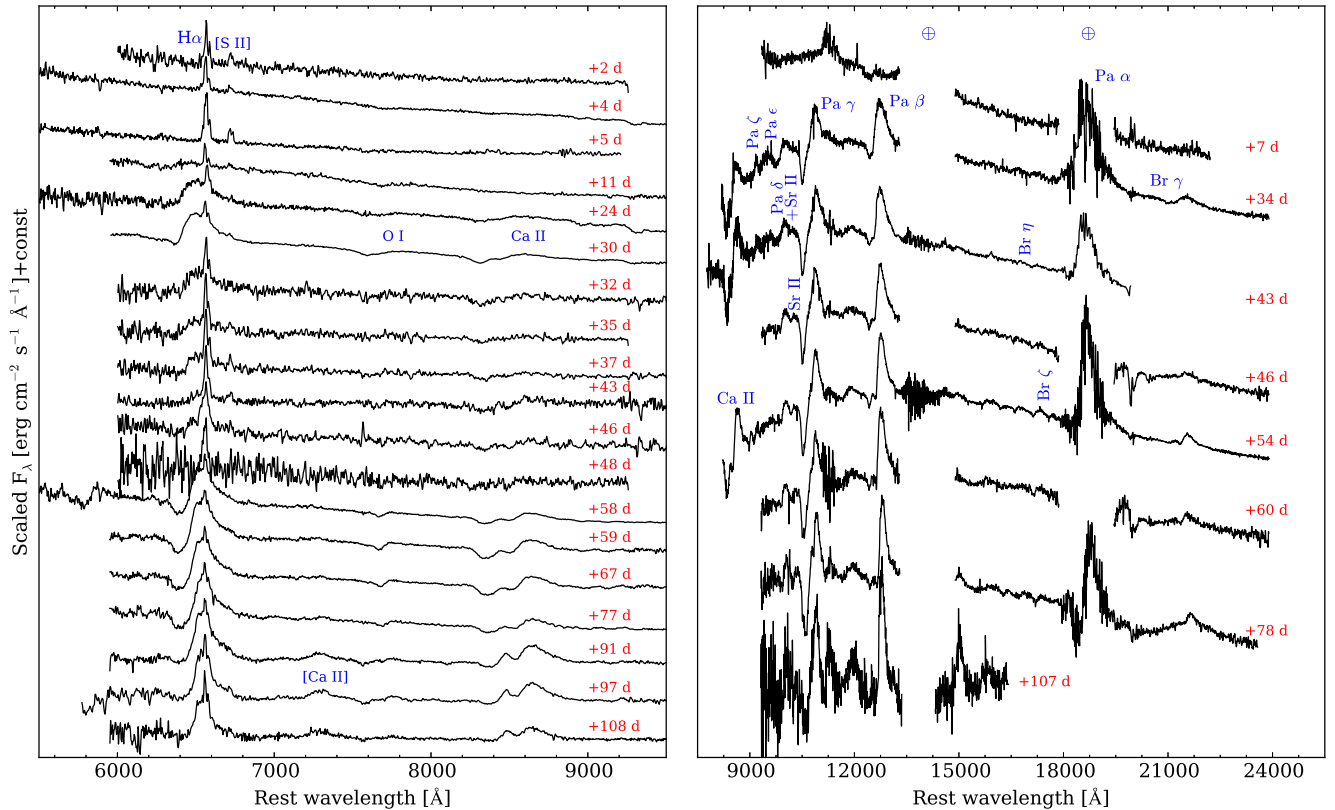


Figure 3. **Left:** Optical and **Right:** NIR spectral sequence of DLT16am. Phases refer to the epoch of the explosion. \oplus symbols mark the positions of the main absorption telluric features. Optical spectra have been corrected for total extinction and redshift. The positions of the main lines are marked. NIR spectra have not been corrected for the total extinction to highlight shallower spectroscopic features.

GROND frames were performed as in Krühler et al. (2008), while the final magnitudes for GROND, IO:O, ALFOSC and Swope frames were obtained using the reduction pipeline SNOOPY⁴. All these images were template subtracted and photometry was calibrated to the AAVSO Photometric All-Sky Survey (APASS⁵) catalog.

DLT16am was also observed in the framework of the CHilean Automatic Supernova sEarch (CHASE) survey (Pignata et al. 2009) in Johnson-Cousins R filters using the PROMPT1 telescope (Reichart et al. 2005). All images were reduced following standard procedures, including dark (with the same exposure time) and flat-field corrections and then template subtracted. The computed photometry is relative to a local sequence calibrated in the field of NGC 1532. The PROMPT1 Johnson-Cousins R -band magnitudes were transformed to the Sloan r -band following the procedure reported in Pignata et al. (2008).

Unfiltered data were provided by the DLT40 (see Section 2) SN search using the 0.4 m PROMPT5 telescope (Reichart et al. 2005), template subtracted and calibrated to the APASS r -band.

DLT16am exploded in the same host and ~ 2 weeks after the Type Ic SN 2016iae (Jha et al. 2016) and pre-SN V -band acquisition images of the field were obtained during its PESSTO spectroscopic campaign. These data were used to constrain the explosion epoch and are included in the V -band light curve of DLT16am (see Smith et al. 2016 and Section 5).

JHK data were also provided by the Public ESO Spectroscopic Survey for Transient Objects (PESSTO⁶) using the 3.58 m New Technology Telescope (NTT) with the Son Of ISAAC camera (SOFI; Moorwood et al. 1998) and reduced using their dedicated pipeline (see Smartt et al. 2015) and the NOT Unbiased Transient Survey (NUTS⁷) with the NOT near-infrared Camera

⁴ <http://sngroup.oapd.inaf.it/snoopy.html>

⁵ <https://www.aavso.org/apass>

⁶ <http://www.pessto.org>

⁷ <http://csp2.lco.cl/not/>

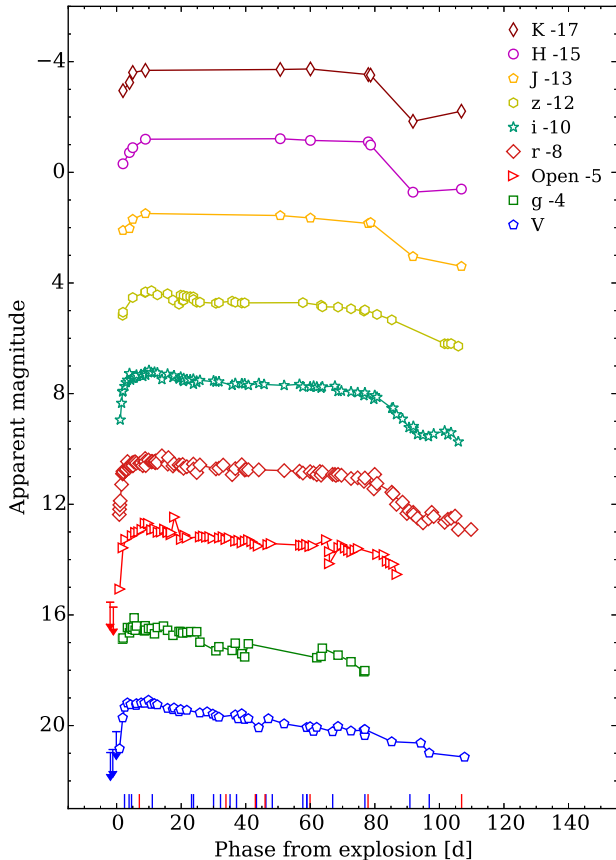


Figure 4. Multi band light curves of DLT16am from the optical to the NIR. Blue ticks mark the epochs at which optical spectra were obtained, while red ticks those of the NIR spectra. *BVJHK* and *griz* magnitudes were calibrated to the Vega and to the AB photometric system, respectively. Phases refer to the estimated epoch of the explosion (see Sections 1 and 5 for details). Magnitudes were not corrected for MW or host extinction. Main pre-discovery limits are reported for *V*-band and unfiltered light curves.

and spectrograph (NOTCam). Pre-reduction steps for NOTCam data were obtained with a modified version of the external IRAF package NOTCAM (v.2.5⁸). In addition to differential flat-fielding and corrected using the median of the sky level at the time of the observations, a bad pixel masking and distortion correction were applied before stacking dithered images. Magnitudes were obtained from pre-reduced images using a dedicated pipeline (FOSCGUI⁹). NIR photometry was calibrated to the Two Micron All-Sky Survey (2MASS¹⁰) catalog, through point-spread-function (PSF) fitting techniques.

⁸ <http://www.not.iac.es/instruments/notcam/guide/observe.html#reductions>

⁹ <http://sngroup.oapd.inaf.it/foscgui.html>

¹⁰ <https://www.ipac.caltech.edu/2mass/>

DLT16am was also observed with *Swift*/XRT on 2016 November 25 (for 2889.4 s), November 26 (for 2966.8 s), November 28 (for 1023.9 s) and December 1 (for 2936.8 s). A previous *Swift*/XRT exposure of SN 2016iae (which is in the same galaxy) was used to extract the background in the region of DLT16am. Due to this complicated background, we obtained a limiting count rate (assuming an 18'' radius) of 1.67×10^{-3} counts s^{-1} . Assuming a power-law model with a photon index of 2 and a Galactic absorption 1.58×10^{20} cm^{-2} (Kalberla et al. 2005), this corresponds to an unabsorbed flux $< 4.1 \times 10^{-14}$ $erg\ cm^{-2}\ s^{-1}$ (0.4–5 keV) and an approximate luminosity of $< 1.9 \times 10^{39}$ $erg\ s^{-1}$ at 20 Mpc (see Section 4). We could not detect DLT16am in UVOT frames, due to the high extinction in the direction of DLT16am (see Section 4.1).

4. THE HOST GALAXY

NGC 1532, the host of DLT16am, is a SB(s)b edge-on galaxy (de Vaucouleurs et al. 1991), located at RA=04:12:04.3, Dec= $-32:52:27$ [J2000], with an apparent total magnitude of $B = 10.65 \pm 0.09$ mag (Lauberts et al. 1989), showing prominent dust lanes close to the position of DLT16am. From our X-shooter spectrum obtained on 2016 December 22, we infer an heliocentric velocity of $1367\ km\ s^{-1}$ ($z = 0.00456$, see Section 6.1), estimated from the average positions of the Balmer emission lines. Throughout the paper we will adopt a distance of 20.0 ± 1.8 Mpc (Tully et al. 2013) to NGC 1532 (leading to a projected distance of $\simeq 8.4$ kpc from the center of the host for DLT16am), although a wide range of values are reported in the literature, suggesting a larger uncertainty. In Section 7, we will show that this value, along with the derived extinction (see Section 4.1), gives absolute magnitudes, pseudo-bolometric luminosities, and hence an estimated ^{56}Ni mass consistent with other distance and reddening-independent quantities.

4.1. Extinction estimate

While for the foreground Galactic extinction we assumed $A_V = 0.042$ mag, as derived from the Schlafly & Finkbeiner (2011) IR-based dust map, the determination of the host reddening in the direction of DLT16am proved to be more complicated. Early spectra of DLT16am exhibit a very red continuum, with low or almost no signal at wavelengths < 6000 Å (with the exception of very early phases, $T \lesssim 5$ d, see Section 6.1), a signature of very high reddening in the direction of the transient.

In order to get an estimate of the host galaxy reddening, we measured the equivalent widths (EWs) of the

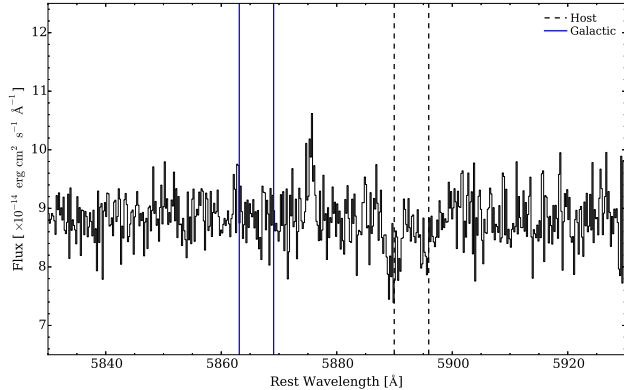


Figure 5. Zoom-in of the region of the Na ID doublet in our X-shooter spectrum. The positions of the host and Galactic Na ID lines are marked with black dashed and blue solid lines, respectively.

Na ID doublet in our X-shooter spectrum (see Figure 5), on the basis of the correlation between the strength of the Na ID $\lambda\lambda 5890, 5896$ absorption and the color excess (see Poznanski et al. 2012; Phillips et al. 2013).

The estimated values ($EW_{D1} \simeq 1.7 \text{ \AA}$, $EW_{D2} \simeq 2.5 \text{ \AA}$) are significantly larger than the saturation limit, where the relation flattens ($EW \gtrsim 0.2 \text{ \AA}$; see Poznanski et al. 2012). We therefore estimated the reddening by matching the colors of DLT16am, during the plateau phase, with those of other Type II SNe (i.e. SNe 2013ej, 2013ab, 2013by and 2014cx; Valenti et al. 2014; Bose et al. 2015; Valenti et al. 2015; Huang et al. 2016, respectively, see Figure 6). These transients were selected among those with similar plateau lengths and observed using similar filters and, for the same reasons, used throughout the paper as comparison objects.

During the plateau phase, the outer hydrogen layer starts to recombine as its temperature decreases to $\sim 6000 \text{ K}$, until the recombination front reaches its base and the plateau ends. This recombination temperature of hydrogen is relatively insensitive to density and metallicity and hence during the plateau SNe II typically share similar physical conditions (see, e.g., Schmidt et al. 1992). A scatter in their colors may therefore be attributed to extinction rather than other intrinsic behaviors (see, e.g., Faran et al. 2014b, and references therein). We therefore fitted the color excess $E(B - V)$ to match the available colors ($g - r$, $r - i$, $V - r$ and $V - i$) of the comparison objects (hereafter ‘references’) within the plateau phase, after correcting the observed colors of the references for the corresponding total extinction. A set of values were obtained comparing the colors of DLT16am to those of each reference, taking the minima of the χ^2 distributions obtained for

each color (i.e. $\chi^2 = \sum_k \frac{1}{\sigma_k^2} (col_{k,ref} - col_{k,DLT16am})^2$, where σ_k^2 are the errors on the colors of DLT16am, and $k = g - r, r - i, V - r, V - i$).

Different extinction laws were recently proposed after analyzing heavily extinguished objects (see, e.g., the case of the obscured Type Ia SN 2002cv Elias-Rosa et al. 2008). Following Calzetti et al. (2000) we also tested their proposed extinction law with $R_V = 4.05 \pm 0.80$, getting a reasonable fit to the colors of the references, but unusual bright absolute peak magnitudes for DLT16am, although still within the combined errors on the reddening and distance. For this reason, we cannot rule out a different extinction law for the environment of DLT16am, although we remark that changing R_V did not significantly improve the result of the fit. Hereafter, we will therefore adopt a standard value ($R_V = 3.1$; Cardelli et al. 1989). Averaging the best fit values obtained using the different references we find $E(B - V) = 1.95 \pm 0.15 \text{ mag}$. A comparable value was obtained measuring the Balmer decrement (i.e. $E(B - V) = 2.0 \text{ mag}$ through the $H\alpha/H\beta$ flux ratio) from our X-shooter spectrum, assuming a case B recombination ratio and a standard extinction law with $R_V = 3.1$ (see, e.g., Botticella et al. 2012).

In Figure 6 we show the resulting color evolution and absolute magnitudes of DLT16am compared with those of the references. We find color evolutions comparable with those of the models, while DLT16am shows brighter absolute magnitudes than those displayed by other objects (although similar to those observed in SN 2013by). In Section 7 we will show that the derived absolute magnitude is consistent with the photospheric expansion velocity derived from the spectroscopic analysis, matching the existing luminosity-velocity relation for SNe II.

4.2. Metallicity and star formation rate

After correcting our X-shooter UVB and VIS spectra for the foreground Galactic extinction, redshift (using the values reported above) and host galaxy extinction, we estimated the local metallicity and star formation rate (SFR) of NGC 1532 at the position of DLT16am. An identification of the host galaxy lines commonly used in the literature is reported in Figure 7.

Using the calibration of Pilyugin & Mattsson (2011), based on the strong emission lines of O^{++} , N^+ and S^+ (the NS calibration), we estimate a local metallicity of $12 + \log(O/H) = 8.45 \text{ dex}$ or $12 + \log(N/H) = 7.46 \text{ dex}$, while following Pettini & Pagel (2004), we obtain $12 + \log(O/H) = 8.67 \text{ dex}$ and 8.84 dex using the $N2$ (Denicoló et al. 2002) and their redefinition of the $O3N2$ (Alloin et al. 1979) indices, respectively. Assuming a solar value of $12 + \log(O/H) = 8.69 \text{ dex}$

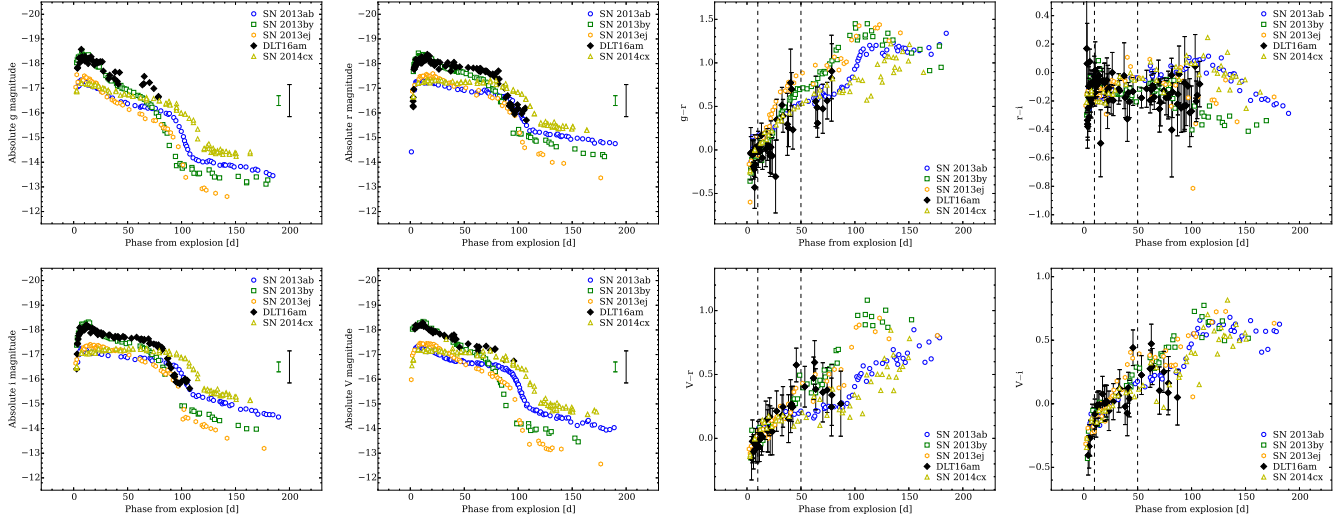


Figure 6. Absolute g , V , r and i -band light curves (left) and $g-r$, $r-i$, $V-r$, $V-i$ color curves (right) of DLT16am adopting a contribution of $E(B-V) = 1.95 \pm 0.15$ mag from the host galaxy to the total extinction. Absolute light and color curves of the models adopted to infer the host extinction (see the text for more details) are also shown for comparison. The representative error bar at +200 d and -16 mag in the absolute curve panels corresponds to the uncertainty on the derived extinction in the direction of DLT16am, while the green errorbar corresponds to the uncertainty on the distance modulus. Dashed black vertical lines in the color curves delimit the region where the colors of DLT16am were fitted to the references (see the text for additional details).

(Asplund et al. 2009), these correspond to $\sim Z_{\odot}$, which is larger than the mean values found by Anderson et al. (2016) for a sample of Type II SNe, and might be even higher, since metallicity values estimated through line diagnostic are believed to underestimate local abundances (see, e.g., López-Sánchez et al. 2012).

Following Rosa-González et al. (2002), we derive the local SFR from the luminosities of $H\alpha$, using the relation given by Kennicutt et al. (1994):

$$SFR(H\alpha)(M_{\odot} \text{ yr}^{-1}) = 7.9 \times 10^{-42} L_{H\alpha} (\text{erg s}^{-1}). \quad (1)$$

Accounting for the derived distance of NGC 1532, we obtain a local SFR of $1.64 \times 10^{-1} M_{\odot} \text{ yr}^{-1}$.

5. PHOTOMETRY

Roughly 2 weeks before the discovery of DLT16am, the Type Ic SN 2016iae exploded in NGC 1532 (Tonry et al. 2016). Pre-SN images of DLT16am were collected during the photometric follow-up campaign of SN 2016iae carried out with the Las Cumbres Observatory 1 m telescope network and these provided the template images used in our photometric analysis. GROND data and NTT acquisition images of SN 2016iae were used as templates for frames obtained with the same instrumental setup.

Prior to the discovery on 2016-11-21.19 UT (Tartaglia et al. 2016b), the last DLT40 non-detection was on 2016-11-19.19 UT ($R > 20.7$ mag), suggesting $\text{JD} = 2457712.7 \pm 1.0$ d as the explosion epoch for DLT16am. On the other

hand, after the initial discovery, (Smith et al. 2016) reported previous detections of the transient on PESSTO V -band acquisition images of SN 2016iae. Although they report a marginal detection on 2016-11-20.10 UT ($\text{JD} = 2457712.6$) analyzing these archival images we could not find any point source within $\sim 3''$ from the position of DLT16am, while we clearly detected the transient on 2016-11-21.10 UT ($\text{JD} = 2457713.6$). Since the detection limit in the frame obtained on November 20.10 UT is not deep enough to rule out the presence of the transient at this time ($V > 20.2$ mag), we will assume 2457712.6 ± 1.0 d as explosion epoch, and refer to this date in computing the phases in both our photometric and spectroscopic analysis.

The final apparent light curves are shown in Figure 4, while Figure 6 shows the absolute and color curves obtained after correcting for the host galaxy extinction (see Section 4.1). Due to the high extinction [$E(B-V) = 1.95 \pm 0.15$ mag see Section 4.1], DLT4016am was never detected in the B band during the first ~ 60 d after the explosion, while early detections covering the rise to the light curve maximum at redder wavelengths were available. At early phases, the light curves show relatively fast rises to the maximum in all bands, after which they set on a plateau-like phase with roughly constant magnitudes up to $\simeq +80$ d.

The early evolution ($\lesssim 10$ d) of the $g-r$, $r-i$, $V-r$ and $V-i$ colors is fast, suggesting a rapid temperature

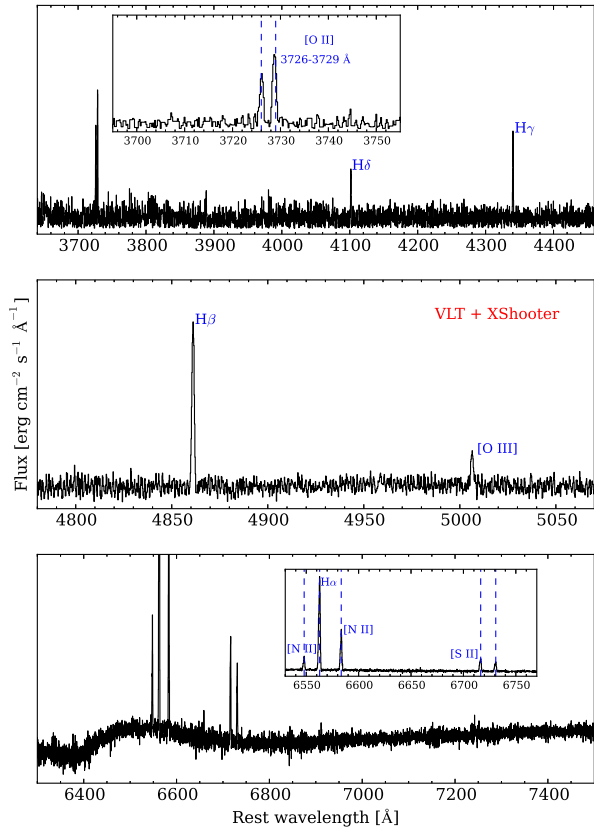


Figure 7. UVB and VIS X-shooter spectra obtained on 2016 December 22. Narrow lines emitted by the host galaxy are identified. Insets in top and bottom panels show zoom-ins around the main spectral features.

evolution (see also Section 6), supporting our claim that DLT16am was discovered soon after the explosion.

The pseudo-bolometric light curve of DLT16am was computed converting the available magnitudes to flux densities at the corresponding effective wavelengths, subsequently integrating using Simpson’s rule. The resulting light curve is shown in Figure 8, along with those of other SNe computed following the same prescriptions and using similar filters. From the analysis of the bolometric light curve of DLT16am, we infer a peak luminosity of $\log L \simeq 43 \text{ erg}^{-1} \text{ s}$, which has to be considered a lower limit, since the contribution of the UV flux is, in general, important in early SN light curves. On the other hand, at later times (e.g. on the radioactive-decay tail) UV bands give a minor contribution to the total flux. We can therefore use the pseudo-bolometric light curve to infer the ^{56}Ni mass produced during the SN explosion. This quantity is generally estimated using the method described in Spiro et al. (2014), taking the bolometric luminosity of SN 1987A during the nebular phase as a reference.

We therefore extrapolated the pseudo-bolometric light curve of DLT16am assuming a complete trapping of the γ -rays produced by the ^{56}Co decay ($\simeq 1 \text{ mag}/100 \text{ d}$). Starting from the last observed point (which is likely a few days after the onset of the radioactive tail), we compared the extrapolated luminosity at $\simeq +150 \text{ d}$ with that of SN 1987A computed using the same integration limits and at the same phase, to get a rough estimate of the mass of radioactive ^{56}Ni deposited in the SN ejecta. Using the relation:

$$M(^{56}\text{Ni}) = 0.075 M_{\odot} \times L_{SN}(t)/L_{87A}(t), \quad (2)$$

we infer a relatively high ^{56}Ni mass of $0.208 \pm 0.044 M_{\odot}$. A similar amount of radioactive ^{56}Ni was derived for the Type II-P SN 1992am (Schmidt et al. 1994), while a larger limit is given for SN 2009kf ($M_{56\text{Ni}} < 0.4 M_{\odot}$; see Botticella et al. 2010). Although the derived luminosity might be significantly affected by the large uncertainty on the estimated extinction, we remark that the photospheric expansion velocity inferred from the spectroscopic analysis is in agreement with the derived bright absolute i -band magnitude (and hence the derived total reddening) for DLT16am, according to the existing luminosity-velocity relation (Hamuy & Pinto 2002) for SNe II (see Section 7). In addition, also the derived ^{56}Ni mass seems to be in agreement with the trend followed by Type II SNe with comparable photospheric velocities and absolute magnitudes (see Hamuy 2003a).

6. SPECTROSCOPY

Our spectroscopic follow-up campaign started on 2016 November 22.64 UT ($\simeq 2 \text{ d}$ after the explosion), lasting up to 2017 March, 7.01 UT (at $\simeq 110 \text{ d}$). NIR spectra were obtained within the same period, with a lower cadence. The flux calibration was checked using photometric information obtained during the closest nights, scaled using low order polynomials.

6.1. Optical spectra

Early spectra are dominated by a nearly featureless and very red continuum, with narrow $\text{H}\alpha$ and $[\text{S II}]$ lines from the host and little or no flux at wavelengths shorter than 5000 \AA . After correcting for the foreground Galactic extinction ($A_V = 0.042 \text{ mag}$), redshift ($z = 0.00456$, inferred from the X-shooter spectrum; see Section 4) and host extinction ($A_V \simeq 6.12 \text{ mag}$), we estimated the temperature of the ejecta at early phases using simple black-body fits to the spectral continuum through the CURVEFIT tool available in the SCIPY¹¹

¹¹ <https://www.scipy.org/>

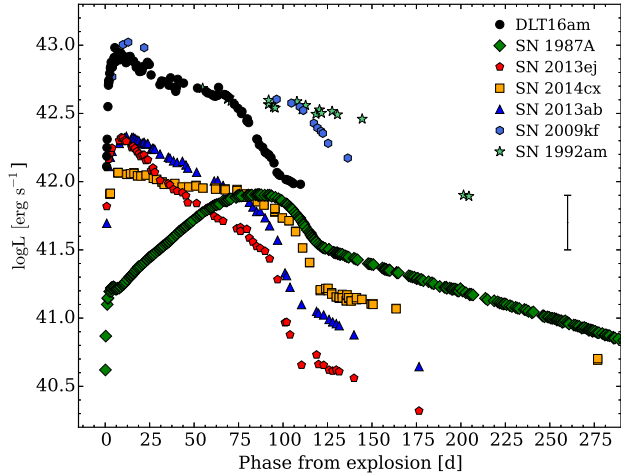


Figure 8. Pseudo-bolometric light curve of DLT16am compared to those of other Type II SNe. Luminosities were obtained using similar filters and integration limits. A representative error bar is also shown, corresponding to the uncertainty on the derived extinction in the direction of DLT16am.

package (Jones et al. 2001–; Van Der Walt et al. 2011). We find a rapid decrease, from 16300 ± 6600 K at +2 d to 10600 ± 3200 K at +5 d, in agreement with the fast color evolution within the early phases (see Section 5), although the large uncertainties might suggest a lack of clear evolution in temperature. The errors on the derived temperatures were estimated by applying different extinction values, within the range of the derived uncertainty on the reddening (see Section 4.1). At later phases ($t > +5$ d), we could not determine the temperatures, since no contribution from the SN to the spectral continuum at $\lambda < 6000 \text{ \AA}$ was observed due to the high extinction (see Section 4.1).

Figure 9 (left panel) shows the results of the black body fit to the spectra up to $\simeq +5$ d. As discussed by Rabinak & Waxman (2011), the time scale of the cooling phase subsequent to the SN shock breakout heating of the progenitor envelope, strongly depends on the initial progenitor properties, such as its radius, density profile, opacity and composition. Using their formalism (i.e. their equation 12), we infer a rough estimate of the progenitor radius fitting the temperature evolution of DLT16am during the first $\simeq 5$ d of its spectroscopic evolution (see Rabinak & Waxman 2011) and (Rubin & Gal-Yam 2017, for an analysis on the limitations of analytic models). Figure 9 (right panel) shows the resulting fit (obtained assuming an explosion energy of 10^{51} erg and a typical optical opacity for a H-rich gas, $\kappa = 0.34 \text{ cm}^2 \text{ g}^{-1}$; Rabinak & Waxman 2011), along

with the temperature evolution obtained for other Type II SNe.

Direct imaging in deep pre-SN archival images confirmed the claim that the majority of SNe II have red super-giant (RSG) progenitors (see, e.g., Maund et al. 2005; Smartt 2009; Fraser et al. 2011; Van Dyk et al. 2012b,a). We therefore adopt the typical mass range for RSG progenitors ($8 - 17 M_{\odot}$; Smartt 2009), and using the Rabinak & Waxman (2011) formalism we obtain a radius of $30 - 660 R_{\odot}$ for the progenitor of DLT16am, where the uncertainty is largely due to the error on the estimated reddening. Although the the model is weakly dependent on the mass of the progenitor (see Rabinak & Waxman 2011), the large uncertainty on the derived temperatures does not allow us to rule out a blue super-giant (BSG) star as a viable progenitor for DLT16am.

From +24 d a broad Full-Width-at-Half-Maximum - FWHM $\simeq 9000 \text{ km s}^{-1}$) $H\alpha$ feature in emission starts to dominate the flux, masking the presence of the host [S II] lines, with blue-shifted peaks typical of Type II SNe (see Anderson et al. 2014a, for a discussion). Following Anderson et al. (2014a) and Gutiérrez et al. (2014), we measure the $H\alpha$ blue-shifted emission offset and the ratio between the EWs of its absorption and emission P-Cygni components (a/e). We find a significant blue-shifted $H\alpha$ peak ($V \simeq 3300 \text{ km s}^{-1}$) at +30 d and a small contribution of the absorption component to the $H\alpha$ P-Cygni profile ($a/e \simeq 0.06$), both indicative of fast declining light curves during the plateau phase and in agreement with the results of our photometric analysis (see Section 7). From the same phase we also detect the NIR (8498, 8542, 8662 \AA) Ca II and the O I (7772, 7774, 7775 \AA) triplets, both becoming more evident at later phases. C I $\lambda 9095$ and Mg II $\lambda 9218$ lines appear between +58 and +59 d, while forbidden [Ca II] lines are visible from +91 d, marking the onset of the nebular phase, possibly blended with the [O II] 7319, 7330 \AA doublet. From the same phase we note a significant change in the relative strengths of the Ca II NIR triplet, which is likely caused by the appearance of the nebular [O I] 8446 \AA line.

From the positions of the minima of the P-Cygni absorption profiles we derived an estimate of the expansion velocities for different ions. $H\alpha$ P-Cygni profiles are clearly visible only from +30 d, when we derive an expansion velocity of $\simeq 8700 \text{ km s}^{-1}$, slowly declining to $\simeq 7100 \text{ km s}^{-1}$ at +97 d (see also Figure 10, panel a). While the Fe II $\lambda 5169$ line is generally assumed as a good tracer of the photospheric velocity, we could not detect this line in any of our spectra of DLT16am due to the high extinction (see Section 4.1). We therefore

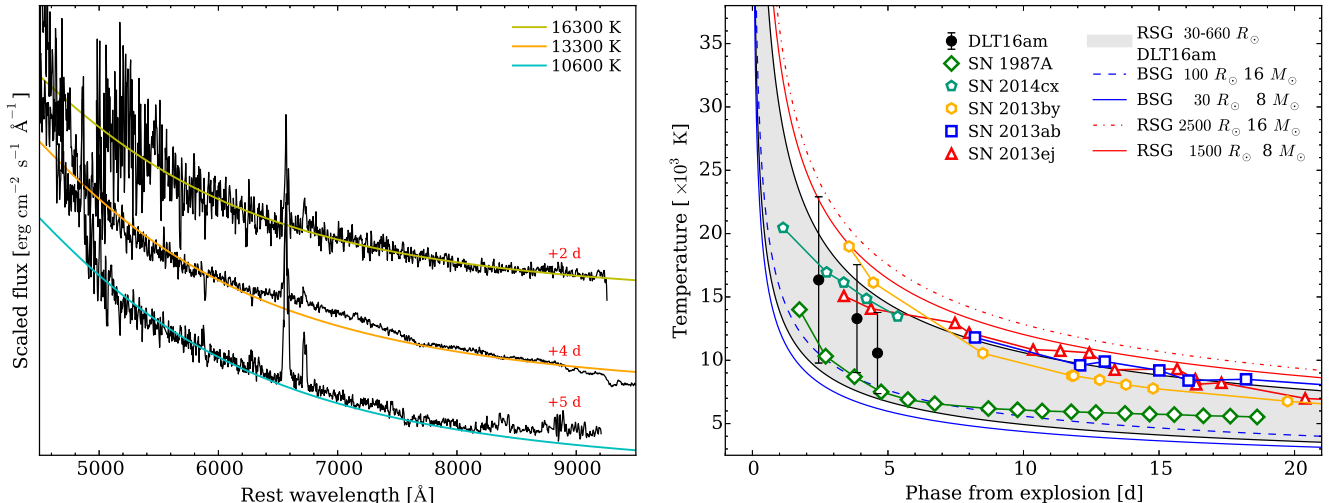


Figure 9. **Left:** Black-body fits to the early spectra of DLT16am. The spectra have been corrected for the derived total extinction in the direction of DLT16am. **Right:** Progenitor radius of DLT16am constrained using the formalism of Rabinak & Waxman (2011). Models for RSGs and BSGs (red and blue lines, respectively) are also shown, while the range of radii obtained for DLT16am is delimited by black lines. Temperature evolutions obtained for other Type II SNe are also shown for comparison.

obtained a rough estimate of the photospheric velocity from the minima of the prominent O I triplet, getting a relatively fast evolution from $\simeq 6300 \text{ km s}^{-1}$ (at +30 d) to $\simeq 3000 \text{ km s}^{-1}$ (at +97 d; see Section 7 and Figure 10 for a detailed discussion). The Ca II NIR triplet was partially resolved, and we inferred an expansion velocity declining from $\simeq 6400 \text{ km s}^{-1}$ to 5000 km s^{-1} for the blend of the 8498,8542 Å lines, and from 7500 km s^{-1} to 3900 km s^{-1} for the 8662 Å line.

6.2. Near infra-red spectra

At +7 d, our SOFI spectrum shows an almost featureless continuum, while at later phases spectra show a significant metamorphosis, as broad H lines with prominent P-Cygni profiles start to dominate the flux. Following the NIR line identifications proposed for SNe 2004et (Maguire et al. 2010) and 1998S (Pozzo et al. 2004), we identify most of the main H Paschen (from Pa α up to Pa ζ) and Brackett (from Br γ up to Br η) lines, although the Pa γ line is most likely a blend with He I (10830 Å). Beginning on +34 d, we also detect the Ca II NIR triplet. We also identify Sr II $\lambda 10327$ in the blue part of the spectra beginning on +43 d, when the feature is still partially blended with the Pa δ line, becoming more evident at later phases.

C I and Mg II lines appear from +54 d, in agreement with the analysis performed on the optical spectra (although we cannot rule out the presence of these lines also at +43 d). From the Pa β absorption minima, we infer an expansion velocity decreasing from $\simeq 8340 \text{ km s}^{-1}$ at +34 d to $\simeq 3460 \text{ km s}^{-1}$ at +107 d, which is consistent with the evolution derived from H α (see above), while

measuring the prominent blue minimum in the blue part of the Pa γ +He I 10830 Å profile, we infer higher expansion velocities, declining from $\simeq 9000 \text{ km s}^{-1}$ to $\simeq 5660 \text{ km s}^{-1}$ from +34 d to +107 d, respectively.

From +43 d we notice a second absorption feature in the blue part of the P-Cygni absorption component of Pa β , becoming more evident at later phases, which might be attributed to a rapidly expanding outer H shell moving at a roughly constant velocity ($9400 - 9500 \text{ km s}^{-1}$). High velocity (HV) components not evolving in time were observed also in the H α profile and He I 10830 Å of other SNe II (see, e.g., the case of SNe 2009bw; Inserra et al. 2012, 1999em and 2004dj; Chakraborti et al. 2012 and the discussion in Chugai et al. 2007) and attributed to weak interaction between the SN ejecta and a pre-existing circumstellar medium surrounding the progenitor star. Analyzing HV components in the H α and He I 10830 Å profiles during the photospheric phase, Chugai et al. (2007) computed a model for ejecta - circumstellar interaction in SNe II-P. Although the expansion velocities inferred from the Pa γ P-Cygni minimum suggest that the entire absorption component might be mainly attributed to the He I 10830 Å line, Figure 11 shows that a similar feature was never observed in the H α profile at any phase, with the possible exception of the +58d spectrum. On the other hand, the signal-to-noise ratio (SNR) of our spectra is not sufficient to safely rule out the presence of this feature at optical wavelengths.

7. COMPARISON WITH OTHER TYPE II SNE

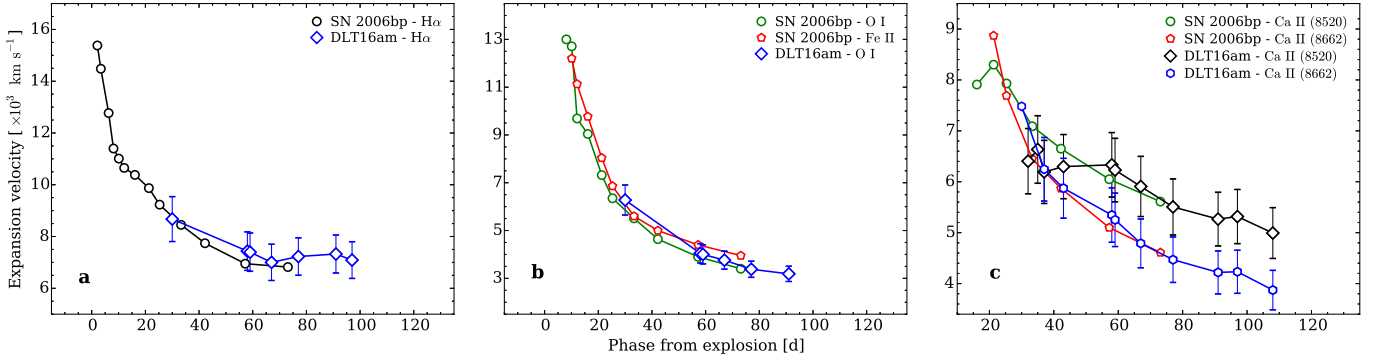


Figure 10. Expansion velocity evolution derived from $H\alpha$ (a), O I $\lambda 7773$ and Fe II $\lambda 5169$ (b) and the NIR Ca II triplet (c), compared to those derived for SN 2006bp. The comparison is made on the basis of the best match of the DLT16am +59 d spectrum obtained with the SNID tool.

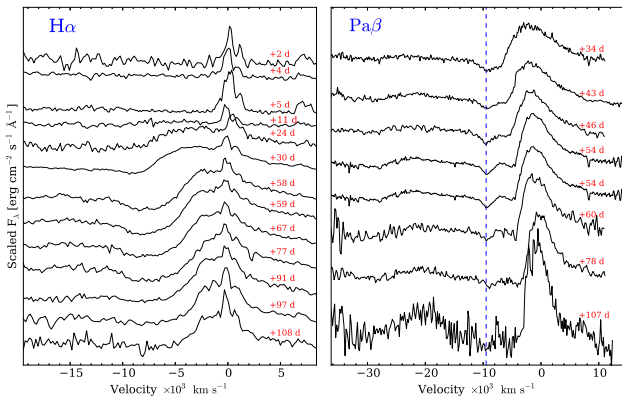


Figure 11. Details of the evolution of the $H\alpha$ and $Pa\beta$ profiles of DLT16am in the velocity space. The position of the blue absorption feature in the $Pa\beta$ profile, with a constant expansion velocity of $9400 - 9500 \text{ km s}^{-1}$ is marked with a dashed blue line. Phases refer to the epoch of the explosion. Spectra with lower SNR are not included.

In Figure 6 we have compared the main photometric properties of a sample of luminous and more canonical Type II SNe. Left panels show that DLT16am is brighter than the normal Type II SNe 2014cx (Huang et al. 2016) and 2013ej (Valenti et al. 2014, although the large uncertainties on the extinction suggest comparable plateau magnitudes), while high luminosities are not unusual among SNe II (see, e.g., the case of SN 2013by; Valenti et al. 2015).

Following the prescriptions of Valenti et al. (2016), we estimate photometric parameters using the V -band photometric evolution. As V -band maximum we consider the point at which the variation in magnitude is less than 0.1 mag d^{-1} , while S_{50V} , the decline rate in $\text{mag}/50\text{d}$ was computed soon after the maximum (10 d after the explosion) to +50 d after the explosion. Figure 12 summarize the results of this analysis, compared to those obtained for other SNe II (Valenti et al.

2016). The V -band maximum for DLT16am occurs on $\text{JD} = 2457719.95$, corresponding to an absolute magnitude $M_V = -18.49 \pm 0.65 \text{ mag}$ (where the error is almost entirely due to the uncertainty on the reddening) and to a relatively fast rise time of $7.4 \pm 1.0 \text{ d}$. At redder wavelengths we find longer rises (10.9, 11.4 and 11.9 d in r -, i - and z -band, respectively), in agreement with the results obtained by González-Gaitán et al. (2015) on a large sample of SNe II. In r band, on the other hand, we find that DLT16am has a relatively slow rise if compared to the sample of Rubin et al. (2016)

Comparing the early-time absolute r -band light curve of SN 2010id with those of SNe 2005cs (Pastorello et al. 2009) and SN 2006bp (Quimby et al. 2007), Gal-Yam et al. (2011) suggested a possible trend for sub-luminous and ‘normal’ events, with faster rises with a sharp onset of the flat plateau for fainter objects, with SN 2006bp showing a more gradual transition over a longer period. Including the slow-rising SNe 2009bw (Inserra et al. 2012) and 2013ej R -band light curves in the comparison, Valenti et al. (2014) also argued that slow rising Type II SNe might be brighter than fast rising transients. The fast rise and the bright absolute magnitude shown by DLT16am seem to contradict these predictions, confirming the results obtained by Rubin et al. (2016) on a sample of R -band light curves of Type II SNe. In Figure 12, left panel, we compare the early V -band absolute light curve of DLT16am with those of a sample of sub-luminous (SNe 2005cs; Pastorello et al. 2009 and 2010id; Gal-Yam et al. 2011), normal (SNe 2006bp; Quimby et al. 2007 and 2013ej Valenti et al. 2014) and luminous (SN 2013by; Valenti et al. 2015 and DLT16am) SNe II, all scaled to the luminosity of the plateau of SN 2010id, in order to gain a better insight into their different rise times. We find a particularly good match with the sub-luminous SN 2005cs, while more luminous transients, like SNe 2006bp and 2013ej,

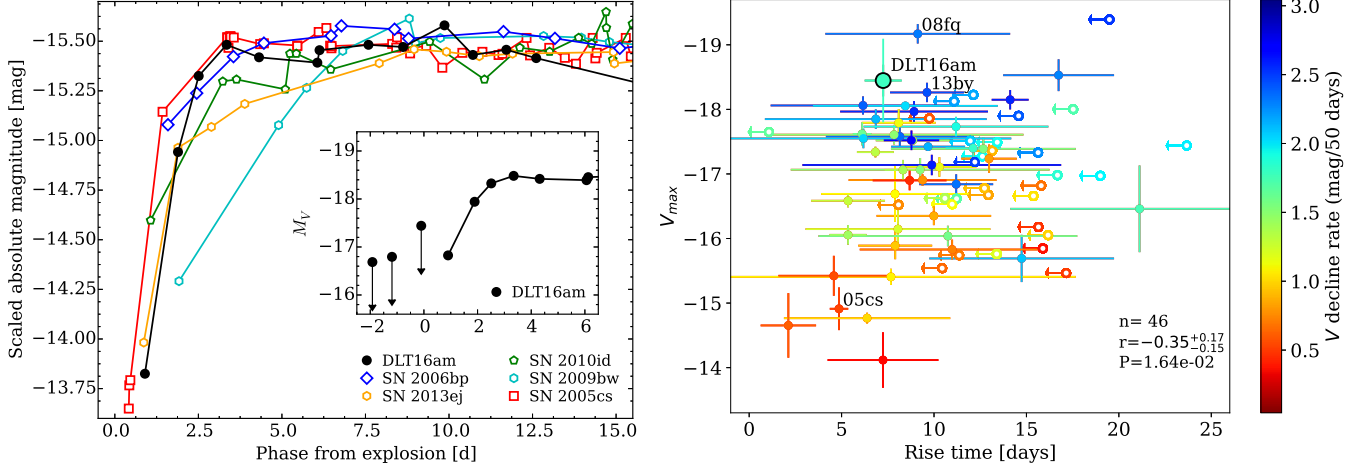


Figure 12. **Left:** Early absolute V -band light curve of DLT16am compared to other Type II SNe (the r -band light curve of SN 2010id is shown for comparison). The light curves are scaled to the plateau luminosity of SN 2010id. Phases refer to the epochs of the explosions. **Right:** V -band absolute magnitude versus rise time for the same sample of SNe II, color-coded according to their V -band decline rate (S_{50V}). n is the number of transients in the plot, r the Pearson s -correlation coefficient and P the probability of detecting a correlation by chance, as in Valenti et al. (2016).

seem to have significantly longer rises to maximum light. This trend is confirmed by the comparison with a larger sample of SNe II shown in Figure 12 (right panel). DLT16am lies close to the brighter end of the absolute peak magnitude range, with a rise time comparable to those displayed by the faintest objects. Comparing the r -band absolute peak magnitude and rise time to the sample of Rubin et al. (2016) (see their Figure 10), on the other hand, we find a longer rise time, while DLT16am falls in a scarcely populated region of their luminosity-rise time diagram. On the other hand, we have to remark that this might be due to the lack of transients with well constrained explosion epochs (see, e.g., the case of SN 2008fq and the large uncertainties in the rise times of the brightest objects).

The historical classification of Type II in II-P and II-L SNe has recently been a matter of debate (see, e.g., Arcavi et al. 2012; Anderson et al. 2014b; Faran et al. 2014b,a; Sanders et al. 2015; Valenti et al. 2016). In order to give an accurate classification of DLT16am, in Figure 13 we compare the V -band light curve of DLT16am to the Type II-P and II-L SNe templates computed by Faran et al. (2014b,a). Although DLT16am shows photometric features typically observed in Type II-P SNe (namely an extended plateau after maximum, with a subsequent steep drop in magnitude around +80 d), like SN 2013by (Valenti et al. 2014) its V -band light curve lies close to the bright end of the II-L templates, in an intermediate region between II-L and II-P templates. This is in agreement with the decline rate derived from the V -band light curve ($S_{50V} = 0.84 \pm 0.04$ mag/50 d), which, according

to Faran et al. (2014a), is greater than the limit for Type II-P SNe (0.5 mag/50 d; see Figure 13). Following Rubin & Gal-Yam (2016) and their proposed classification based on the early light curves morphology, we compare the r -band light curve of DLT16am to the results of their analysis on the sample of Rubin et al. (2016), obtaining a good match with their fast rise–fast decline (II-FF) cluster of Type II SNe.

Figure 14 shows a comparison of our +59 d spectrum with those of other Type II SNe, based on the best fits of the spectral features to archival spectra obtained using the ‘Supernova Identification’ (SNID¹²; Blondin & Tonry 2007) tool. While the best match was obtained with the Type II-P SN 2006bp (Quimby et al. 2007; Dessart et al. 2008), good fits of the spectral features were obtained also with the Type II-P SNe 2004et (Sahu et al. 2006; Misra et al. 2007; Maguire et al. 2010) and 1999em (Hamuy et al. 2001; Leonard et al. 2002; Elmhamdi et al. 2003; Dessart & Hillier 2006). Based on this similarity, we compared the expansion velocities of DLT16am with those obtained for SN 2006bp, obtaining similar values for all the ions visible in both set of spectra (see Figure 10). Due to the high extinction, we could not compare the expansion velocities inferred from Fe II (5169 Å) or Sc II (6246 Å), which are typically considered good indicators of the photospheric velocity. On the other hand, SN 2006bp shows similar Fe II (5169 Å) and O I (7773 Å) expansion velocities (see Figure 10, panel b) and based on

¹² <https://people.lam.fr/blondin.stephane/software/snid/>

the strong spectroscopic similarities between the two transients, we can therefore use the velocity evolution inferred from the O I minima as a rough estimate of the photospheric expansion velocity for DLT16am. Using the existing luminosity-velocity relation for Type II SNe (Hamuy & Pinto 2002; Hamuy 2003b) we can therefore perform an independent consistency check on the derived host galaxy reddening in the direction of DLT16am (see Section 4.1). Hamuy & Pinto (2002) use +50 d as an indicative epoch (roughly the mid point of the plateau phase) and, although DLT16am shows a relatively short plateau lasting $\simeq 80$ d, we will adopt the same approach, comparing the expansion velocity and absolute V -magnitude with those obtained from the sample of Hamuy (2003b) at similar phases. A similar approach was adopted also for the absolute V -band luminosity, where we took the uncertainty on the distance modulus and the total extinction as an estimate of the error on the derived magnitude. In Figure 15 we compare the results for DLT16am with those obtained for the sample of Hamuy (2003b). With a photospheric velocity of $\simeq 4585 \text{ km s}^{-1}$ and an absolute V -band magnitude at +50 d of $M_V = -17.40 \pm 0.65 \text{ mag}$, DLT16am falls in the region of other luminous SNe II, in agreement with the expectation that luminous transients have higher expansion velocities (see also Rubin et al. 2016). The correlation between absolute peak magnitudes and expansion velocity was recently confirmed by Gutiérrez et al. (2017), who also confirmed the previous claim of Anderson et al. (2014a) and Valenti et al. (2016) that brighter SNe II show shorter plateau phases and steeper decline rates. Similar results were also reported by Galbany et al. (2016) analyzing the light curves of a large sample of Type II SNe.

8. SUMMARY AND CONCLUSIONS

We have discussed the results of our analysis on the photometric and spectroscopic data obtained during our follow-up campaign of the Type II SN DLT16am (aka SN 2016ija). The transient was discovered during the ongoing DLT40 survey, which is monitoring a sample of galaxies in the nearby Universe in search for young SNe within the first days from the explosion.

Early spectra showed a highly reddened, nearly featureless continuum, while H, Ca II and O I lines with prominent P-Cygni profiles gradually appear at later phases. The comparison of the colors of DLT16am with those of other similar transients during the plateau phase suggests a contribution of $E(B - V) = 1.95 \pm 0.15 \text{ mag}$ from the host galaxy (NGC 1532) to the total extinction (see Section 4.1 and Figure 6). Although DLT16am was clearly detected by our survey

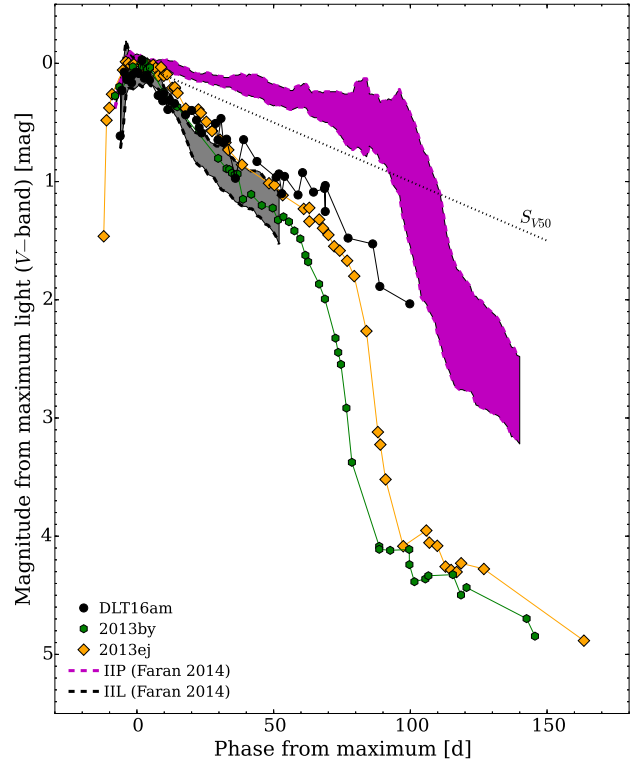


Figure 13. Absolute V -band light curve of DLT16am and other similar transients compared with templates computed by Faran et al. (2014b,a) for Type II SNe. The dotted black line marks the limiting slope (S_{50V} ; see the text for details) between Type II-P (magenta dashed lines) and II-L (black dashed models) SNe.

at redder optical wavelengths, its substantial extinction of $A_V \simeq 6 \text{ mag}$ supports the claim that optical surveys might be missing a significant fraction of nearby, highly reddened SNe (e.g. Mattila et al. 2012; Jencson et al. 2017). Other examples of recent heavily obscured CCSNe observed in nearby galaxies include SN 2009hd (Elias-Rosa et al. 2011), SN 2005at (Kankare et al. 2014a) and SN 2013fc (Kangas et al. 2016), SPIRITS 15c and SPIRITS 14buu; Jencson et al. 2017, or SNe 2008cs, 2011hi, and 2010P Kankare et al. 2008, 2012, 2014b). Such events can have important implications for the comparison between CCSN rates and the cosmic star formation history.

Assuming a standard ($R_V = 3.1$) extinction law (Cardelli et al. 1989) and a distance modulus $\mu = 31.51 \pm 0.20 \text{ mag}$ (Tully et al. 2013), we obtain a relatively bright absolute peak magnitude ($M_V = -18.49 \pm 0.65 \text{ mag}$) compared to those displayed by other Type II-P-like SNe.

The absolute magnitude at +50 d is consistent with the photospheric velocity inferred at the same phase, according to the existing luminosity-velocity relation for

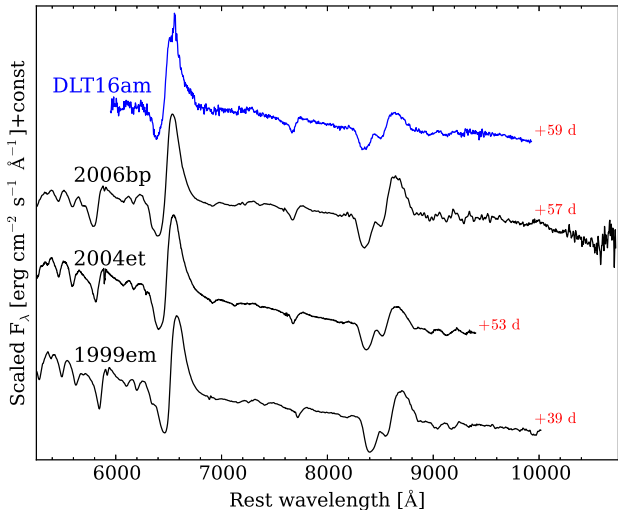


Figure 14. Comparison of the +59 d spectrum of DLT16am with those of a sample of Type II SNe at similar phases. Comparison objects were selected on the basis of the results obtained using the SNID comparison tool (Blondin & Tonry 2007). Fluxes have been scaled to arbitrary constants.

Type II SNe (see Hamuy & Pinto 2002; Hamuy 2003b, and Figure 15). The derived slope within 50 d from the explosion (S_{50V} ; see Section 7) suggests a relatively steep decline during the plateau phase ($S_{50V} = 0.84 \pm 0.04$ mag/50 d), which, according to Faran et al. (2014a) (who give a limit of 0.5 mag/50 d to the maximum slope for SNe II-P), means that DLT16am should be considered a Type II-L SN. A similar conclusion was reached by Valenti et al. (2014) in their analysis of SN 2013by, which, like DLT16am, showed an extended plateau, with a drop in magnitude around 80 d after the explosion (see also Figure 6).

In Figure 12 we have shown a comparison of the fundamental photometric parameters inferred for DLT16am with those obtained for a sample of SNe II. The fast rise time (7.4 ± 1.0 d) and the bright V -band absolute magnitude at maximum ($M_V = -18.49 \pm 0.65$ mag) seem to contradict the prediction that luminous Type II SNe have long rise times compared to those of sub-luminous events. The lack of other Type II SNe in the region where DLT16am falls highlights its peculiarity, but might also be due to the lack of transients with well constrained explosion epochs.

It is therefore crucial to increase our sample of SNe II with well constrained explosion epochs and rise times, providing early discoveries and subsequent multi-wavelength data. With its estimated rate of $\simeq 4 - 5$ SNe II per year discovered within 1 d from the explosion, confirmed by the number of discoveries during the first year of operations, the DLT40 survey will signifi-

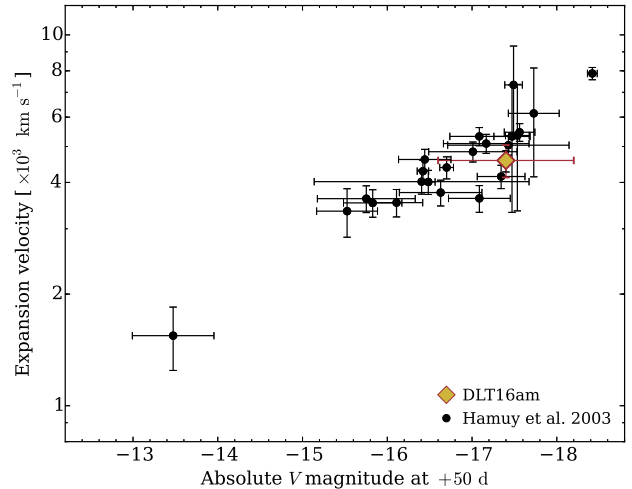


Figure 15. Expansion velocity (inferred from Fe II $\lambda 5169$ absorption minima) versus V -band absolute magnitude for a sample of SNe II. Velocities and luminosities have been computed 50 d after the explosion (roughly the mid-point of the plateau phase; see Hamuy et al. 2001). DLT16am is marked with a yellow and red diamond.

cantly increase the number of early discoveries, helping to further explore correlations between fundamental parameters of Type II SNe.

Based on observations collected at: The Very Large Telescope operated by the European Organisation for Astronomical Research in the Southern hemisphere, Chile as part of the ESO large programme 198.A-0915.. ESO La Silla Observatory as part of PESSTO (197.D-1075.191.D-0935).

The Gemini Observatory, under program GN-2016B-Q-57, which is operated by the Association of Universities for Research in Astronomy, Inc., under a cooperative agreement with the NSF on behalf of the Gemini partnership: the National Science Foundation (United States), the National Research Council (Canada), CONICYT (Chile), Ministerio de Ciencia, Tecnología e Innovación Productiva (Argentina), and Ministério da Ciência, Tecnologia e Inovação (Brazil).

Based on observations made with the Nordic Optical Telescope, operated by the Nordic Optical Telescope Scientific Association at the Observatorio del Roque de los Muchachos, La Palma, Spain, of the Instituto de Astrofísica de Canarias.

This paper includes data gathered with the 6.5 meter Magellan Telescopes located at Las Campanas Observatory, Chile.

This work makes use of observations from the Las Cumbres Observatory network of telescopes.

This work includes data obtained with the Swope Tele-

scope at Las Campanas Observatory, Chile, as part of the Swope Time Domain Key Project (PI Piro, Co-PIs Shappee, Drout, Madore, Phillips, Foley, and Hsiao).

SNOoPy is a package for SN photometry using PSF fitting and/or template subtraction developed by E. Cappellaro. A package description can be found at <http://sngroup.oapd.inaf.it/snoopy.html>.

FOSCGUI is a graphic user interface aimed at extracting SN spectroscopy and photometry obtained with FOSC-like instruments. It was developed by E. Cappellaro. A package description can be found at <http://sngroup.oapd.inaf.it/foscgui.html>.

Research by D.J.S. and L.T. is supported by NSF grant AST-1412504 and AST-1517649.

C.G. acknowledges support from the Carlsberg Foundation.

R.C. and M.S. acknowledge support from STFC grant ST/L000679/1 and EU/FP7-ERC grant no [615929] T.W.C. acknowledges the support through the Sofia Kovalevskaja Award to P. Schady from the Alexander von Humboldt Foundation of Germany.

Part of the funding for GROND (both hardware as well as personnel) was generously granted from the Leibniz-Prize to Prof. G. Hasinger (DFG grant HA 1850/28-1). Support for G.P. is provided by the Ministry of Economy, Development, and Tourism's Millennium Science Initiative through grant IC120009, awarded to The Millennium Institute of Astrophysics, MAS.

J.H. acknowledges financial support from the Finnish Cultural Foundation and the Vilho, Yrjö and Kalle Väisälä Foundation of the Finnish Academy of Science and Letters.

D.A.H., C.M., and G.H. are supported by NSF grant 1313484.

M.D.S. acknowledges support by a research grant

(13261) from the VILLUM FONDEN and for financial support of NUTS by the the Instrument Center for Danish Astrophysics (IDA).

L.G. was supported in part by the US National Science Foundation under Grant AST-1311862.

M.M.P., N.M. and E.Y.H. acknowledge the support provided by the National Science Foundation under Grant No. AST-1008343, AST-1613472 and AST-1613426.

A.G.-Y. is supported by the EU via ERC grant No. 725161, the Quantum Universe I-Core program, the ISF, the BSF Transformative program and by a Kimmel award.

K.M. acknowledges support from the STFC through an Ernest Rutherford Fellowship.

The UCSC group is supported in part by NSF grant AST-1518052, the Gordon & Betty Moore Foundation, and from fellowships from the Alfred P. Sloan Foundation and the David and Lucile Packard Foundation to R.J.F.

Facilities: VLT:Kueyen (X-shooter spectrograph Vernet et al. 2011), NTT (EFOSC2 Buzzoni et al. 1984 and SOFI Moorwood et al. 1998 spectrographs), Gemini:Gillett (GNIRS spectrograph; Elias et al. 2006), NOT (ALFOSC and NOTCam cameras), Magellan:Baade (FIRE spectrograph), FTN, FTS (FLOYDS spectrographs), LCOGT, Swope, Liverpool:2m (IO:O camera), Max Planck:2.2m (GROND camera), CTIO:PROMPT (PROPT5 telescope; Reichart et al. 2005)

Software: SNID (Blondin & Tonry 2007), Foscgui (<http://graspa.oapd.inaf.it/foscgui.html>), SNOoPy (<http://sngroup.oapd.inaf.it/snoopy.html>), PySALT (Crawford et al. 2010b), XDGNIIRS, firehose (Simcoe et al. 2013). ESOREFLEX (Freudling et al. 2013), SciPy (<https://www.scipy.org/>).

REFERENCES

- Alloin, D., Collin-Souffrin, S., Joly, M., & Vigroux, L. 1979, *A&A*, 78, 200
- Anderson, J. P., Dessart, L., Gutierrez, C. P., et al. 2014a, *MNRAS*, 441, 671
- Anderson, J. P., González-Gaitán, S., Hamuy, M., et al. 2014b, *ApJ*, 786, 67
- Anderson, J. P., Gutiérrez, C. P., Dessart, L., et al. 2016, *A&A*, 589, A110
- Arcavi, I., Gal-Yam, A., Cenko, S. B., et al. 2012, *ApJL*, 756, L30
- Arcavi, I., Hosseinzadeh, G., Brown, P. J., et al. 2017, *ApJL*, 837, L2
- Asplund, M., Grevesse, N., Sauval, A. J., & Scott, P. 2009, *ARA&A*, 47, 481
- Barbarino, C., Botticella, M. T., Dall’Ora, M., et al. 2017, *MNRAS*, 471, 2463
- Becker, A. 2015, HOTPANTS: High Order Transform of PSF ANd Template Subtraction, Astrophysics Source Code Library, ascl:1504.004
- Bellm, E. 2014, in The Third Hot-wiring the Transient Universe Workshop, ed. P. R. Wozniak, M. J. Graham, A. A. Mahabal, & R. Seaman, 27–33
- Bersten, M. C., Benvenuto, O. G., Nomoto, K., et al. 2012, *ApJ*, 757, 31
- Bloemen, S., Groot, P., Nelemans, G., & Klein-Wolt, M. 2015, in Astronomical Society of the Pacific Conference Series, Vol. 496, Living Together: Planets, Host Stars and Binaries, ed. S. M. Rucinski, G. Torres, & M. Zejda, 254

- Blondin, S., & Tonry, J. L. 2007, *ApJ*, 666, 1024
- Bloom, J. S., Kasen, D., Shen, K. J., et al. 2012, *ApJL*, 744, L17
- Bose, S., Valenti, S., Misra, K., et al. 2015, *MNRAS*, 450, 2373
- Botticella, M. T., Smartt, S. J., Kennicutt, R. C., et al. 2012, *A&A*, 537, A132
- Botticella, M. T., Trundle, C., Pastorello, A., et al. 2010, *ApJL*, 717, L52
- Bowen, I. S., & Vaughan, Jr., A. H. 1973, *ApOpt*, 12, 1430
- Brown, T. M., Baliber, N., Bianco, F. B., et al. 2013, *PASP*, 125, 1031
- Buzzoni, B., Delabre, B., Dekker, H., et al. 1984, *The Messenger*, 38, 9
- Calzetti, D., Armus, L., Bohlin, R. C., et al. 2000, *ApJ*, 533, 682
- Cao, Y., Kulkarni, S. R., Howell, D. A., et al. 2015, *Nature*, 521, 328
- Cappellaro, E., Botticella, M. T., Pignata, G., et al. 2015, *A&A*, 584, A62
- Cardelli, J. A., Clayton, G. C., & Mathis, J. S. 1989, *ApJ*, 345, 245
- Chakraborti, S., Yadav, N., Ray, A., et al. 2012, *ApJ*, 761, 100
- Chambers, K. C., Magnier, E. A., Metcalfe, N., et al. 2016, *ArXiv e-prints*, arXiv:1612.05560
- Chen, T.-W., Schady, P., & Kruehler, T. 2016, *The Astronomer's Telegram*, 9789
- Chugai, N. N., Chevalier, R. A., & Utrobin, V. P. 2007, *ApJ*, 662, 1136
- Crawford, S. M., Still, M., Schellart, P., et al. 2010a, in *Proc. SPIE*, Vol. 7737, *Observatory Operations: Strategies, Processes, and Systems III*, 773725
- Crawford, S. M., Still, M., Schellart, P., et al. 2010b, in *Proc. SPIE*, Vol. 7737, *Observatory Operations: Strategies, Processes, and Systems III*, 773725
- Dahlen, T., Strolger, L.-G., Riess, A. G., et al. 2012, *ApJ*, 757, 70
- de Vaucouleurs, G., de Vaucouleurs, A., Corwin, Jr., H. G., et al. 1991, *Third Reference Catalogue of Bright Galaxies. Volume I: Explanations and references. Volume II: Data for galaxies between 0^h and 12^h . Volume III: Data for galaxies between 12^h and 24^h .*
- Denicoló, G., Terlevich, R., & Terlevich, E. 2002, in *Revista Mexicana de Astronomía y Astrofísica Conference Series*, Vol. 12, *Revista Mexicana de Astronomía y Astrofísica Conference Series*, ed. W. J. Henney, J. Franco, & M. Martos, 257–257
- Dessart, L., & Hillier, D. J. 2006, *A&A*, 447, 691
- Dessart, L., Blondin, S., Brown, P. J., et al. 2008, *ApJ*, 675, 644
- Elias, J. H., Joyce, R. R., Liang, M., et al. 2006, in *Society of Photo-Optical Instrumentation Engineers (SPIE) Conference Series*, Vol. 6269, *Society of Photo-Optical Instrumentation Engineers (SPIE) Conference Series*, 4
- Elias-Rosa, N., Benetti, S., Turatto, M., et al. 2008, *MNRAS*, 384, 107
- Elias-Rosa, N., Van Dyk, S. D., Li, W., et al. 2011, *ApJ*, 742, 6
- Elmhamdi, A., Danziger, I. J., Chugai, N., et al. 2003, *MNRAS*, 338, 939
- Faran, T., Poznanski, D., Filippenko, A. V., et al. 2014a, *MNRAS*, 445, 554
- . 2014b, *MNRAS*, 442, 844
- Fossey, S. J., Cooke, B., Pollack, G., Wilde, M., & Wright, T. 2014, *Central Bureau Electronic Telegrams*, 3792
- Fraser, M., Ergon, M., Eldridge, J. J., et al. 2011, *MNRAS*, 417, 1417
- Freudling, W., Romaniello, M., Bramich, D. M., et al. 2013, *A&A*, 559, A96
- Fryer, C. L., Ruiter, A. J., Belczynski, K., et al. 2010, *ApJ*, 725, 296
- Gal-Yam, A., Kasliwal, M. M., Arcavi, I., et al. 2011, *ApJ*, 736, 159
- Gal-Yam, A., Arcavi, I., Ofek, E. O., et al. 2014, *Nature*, 509, 471
- Galbany, L., Hamuy, M., Phillips, M. M., et al. 2016, *AJ*, 151, 33
- González-Gaitán, S., Tominaga, N., Molina, J., et al. 2015, *MNRAS*, 451, 2212
- Goobar, A., Kromer, M., Siverd, R., et al. 2015, *ApJ*, 799, 106
- Greiner, J., Bornemann, W., Clemens, C., et al. 2008, *PASP*, 120, 405
- Gutiérrez, C. P., Anderson, J. P., Hamuy, M., et al. 2014, *ApJL*, 786, L15
- . 2017, *ArXiv e-prints*, arXiv:1709.02799
- Hamuy, M. 2003a, *ApJ*, 582, 905
- . 2003b, *ArXiv Astrophysics e-prints*, astro-ph/0309122
- Hamuy, M., & Pinto, P. A. 2002, *ApJL*, 566, L63
- Hamuy, M., Pinto, P. A., Maza, J., et al. 2001, *ApJ*, 558, 615
- Höflich, P., & Stein, J. 2002, *ApJ*, 568, 779
- Horiuchi, S., Beacom, J. F., Kochanek, C. S., et al. 2011, *ApJ*, 738, 154
- Hosseinzadeh, G., Sand, D. J., Valenti, S., et al. 2017, *ApJL*, 845, L11
- Huang, F., Wang, X., Zampieri, L., et al. 2016, *ApJ*, 832, 139

- Insera, C., Turatto, M., Pastorello, A., et al. 2012, *MNRAS*, 422, 1122
- Ivezic, Z., Tyson, J. A., Abel, B., et al. 2008, ArXiv e-prints, arXiv:0805.2366
- Jencson, J. E., Kasliwal, M. M., Johansson, J., et al. 2017, *ApJ*, 837, 167
- Jha, S. W., Foley, R. J., & Skelton, R. 2016, *The Astronomer's Telegram*, 9754
- Jones, E., Oliphant, T., Peterson, P., et al. 2001–, SciPy: Open source scientific tools for Python, [Online; accessed `today`]
- Kalberla, P. M. W., Burton, W. B., Hartmann, D., et al. 2005, *A&A*, 440, 775
- Kangas, T., Mattila, S., Kankare, E., et al. 2016, *MNRAS*, 456, 323
- Kankare, E., Mattila, S., Ryder, S., et al. 2008, *ApJL*, 689, L97
- . 2012, *ApJL*, 744, L19
- Kankare, E., Fraser, M., Ryder, S., et al. 2014a, *A&A*, 572, A75
- Kankare, E., Mattila, S., Ryder, S., et al. 2014b, *MNRAS*, 440, 1052
- Kasen, D. 2010, *ApJ*, 708, 1025
- Kasen, D., Röpke, F. K., & Woosley, S. E. 2009, *Nature*, 460, 869
- Kennicutt, Jr., R. C., Tamblyn, P., & Congdon, C. E. 1994, *ApJ*, 435, 22
- Khazov, D., Yaron, O., Gal-Yam, A., et al. 2016, *ApJ*, 818, 3
- Kochanek, C. S., Shappee, B. J., Stanek, K. Z., et al. 2017, *PASP*, 129, 104502
- Krüehler, T., Küpcü Yoldaş, A., Greiner, J., et al. 2008, *ApJ*, 685, 376
- Lauberts, A., Valentijn, E. A., & Observatory, E. S. 1989, *The surface photometry catalogue of the ESO-Uppsala galaxies (Garching bei Munchen, FRG : European Southern Observatory)*
- Law, N. M., Kulkarni, S. R., Dekany, R. G., et al. 2009, *PASP*, 121, 1395
- Leonard, D. C., Filippenko, A. V., Gates, E. L., et al. 2002, *PASP*, 114, 35
- López-Sánchez, Á. R., Dopita, M. A., Kewley, L. J., et al. 2012, *MNRAS*, 426, 2630
- Maguire, K., Di Carlo, E., Smartt, S. J., et al. 2010, *MNRAS*, 404, 981
- Maoz, D., & Mannucci, F. 2012, *PASA*, 29, 447
- Marion, G. H., Brown, P. J., Vinkó, J., et al. 2016, *ApJ*, 820, 92
- Mattila, S., Dahlen, T., Efstathiou, A., et al. 2012, *ApJ*, 756, 111
- Maund, J. R., Smartt, S. J., & Danziger, I. J. 2005, *MNRAS*, 364, L33
- Mazzali, P. A. 2001, *MNRAS*, 321, 341
- Mazzali, P. A., Sullivan, M., Hachinger, S., et al. 2014, *MNRAS*, 439, 1959
- Melinder, J., Dahlen, T., Mencía Trinchant, L., et al. 2012, *A&A*, 545, A96
- Miller, A. A., Cao, Y., Piro, A. L., et al. 2017, ArXiv e-prints, arXiv:1708.07124
- Misra, K., Pooley, D., Chandra, P., et al. 2007, *MNRAS*, 381, 280
- Moorwood, A., Cuby, J.-G., & Lidman, C. 1998, *The Messenger*, 91, 9
- Nugent, P. E., Sullivan, M., Cenko, S. B., et al. 2011, *Nature*, 480, 344
- Pastorello, A., Valenti, S., Zampieri, L., et al. 2009, *MNRAS*, 394, 2266
- Pettini, M., & Pagel, B. E. J. 2004, *MNRAS*, 348, L59
- Phillips, M. M., Simon, J. D., Morrell, N., et al. 2013, *ApJ*, 779, 38
- Pignata, G., Benetti, S., Mazzali, P. A., et al. 2008, *MNRAS*, 388, 971
- Pignata, G., Maza, J., Antezana, R., et al. 2009, in *American Institute of Physics Conference Series*, Vol. 1111, American Institute of Physics Conference Series, ed. G. Giobbi, A. Tornambe, G. Raimondo, M. Limongi, L. A. Antonelli, N. Menci, & E. Brocato, 551–554
- Pilyugin, L. S., & Mattsson, L. 2011, *MNRAS*, 412, 1145
- Piro, A. L., Muhleisen, M., Arcavi, I., et al. 2017, ArXiv e-prints, arXiv:1703.00913
- Piro, A. L., & Nakar, E. 2014, *ApJ*, 784, 85
- Poznanski, D., Prochaska, J. X., & Bloom, J. S. 2012, *MNRAS*, 426, 1465
- Pozzo, M., Meikle, W. P. S., Fassia, A., et al. 2004, *MNRAS*, 352, 457
- Quimby, R. M., Wheeler, J. C., Höflich, P., et al. 2007, *ApJ*, 666, 1093
- Rabinak, I., & Waxman, E. 2011, *ApJ*, 728, 63
- Reichart, D., Nysewander, M., Moran, J., et al. 2005, *Nuovo Cimento C Geophysics Space Physics C*, 28, 767
- Röpke, F. K., Hillebrandt, W., Schmidt, W., et al. 2007, *ApJ*, 668, 1132
- Rosa-González, D., Terlevich, E., & Terlevich, R. 2002, *MNRAS*, 332, 283
- Rubin, A., & Gal-Yam, A. 2016, *ApJ*, 828, 111
- . 2017, *ApJ*, 848, 8
- Rubin, A., Gal-Yam, A., De Cia, A., et al. 2016, *ApJ*, 820, 33
- Sahu, D. K., Anupama, G. C., Srividya, S., & Muneer, S. 2006, *MNRAS*, 372, 1315

- Sand, D., Wyatt, S., Valenti, S., et al. 2017a, The Astronomer's Telegram, 10343
- Sand, D. J., Valenti, S., Tartaglia, L., et al. 2017b, The Astronomer's Telegram, 10569
- Sanders, N. E., Soderberg, A. M., Gezari, S., et al. 2015, ApJ, 799, 208
- Sapir, N., & Waxman, E. 2017, ApJ, 838, 130
- Schlafly, E. F., & Finkbeiner, D. P. 2011, ApJ, 737, 103
- Schmidt, B. P., Kirshner, R. P., & Eastman, R. G. 1992, ApJ, 395, 366
- Schmidt, B. P., Kirshner, R. P., Eastman, R. G., et al. 1994, AJ, 107, 1444
- Shappee, B. J., Prieto, J. L., Grupe, D., et al. 2014, ApJ, 788, 48
- Simcoe, R. A., Burgasser, A. J., Schechter, P. L., et al. 2013, PASP, 125, 270
- Smartt, S. J. 2009, ARA&A, 47, 63
- Smartt, S. J., Valenti, S., Fraser, M., et al. 2015, A&A, 579, A40
- Smith, K. W., Rodriguez, O., Takats, K., et al. 2016, The Astronomer's Telegram, 9784
- Spiro, S., Pastorello, A., Pumo, M. L., et al. 2014, MNRAS, 439, 2873
- Strolger, L.-G., Dahlen, T., Rodney, S. A., et al. 2015, ApJ, 813, 93
- Tartaglia, L., Hosseinzadeh, G., Arcavi, I., et al. 2016a, The Astronomer's Telegram, 9453
- Tartaglia, L., Sand, D., & Valenti, S. 2016b, The Astronomer's Telegram, 9782
- . 2016c, The Astronomer's Telegram, 9782
- Tartaglia, L., Sand, D., Valenti, S., et al. 2017a, The Astronomer's Telegram, 10058
- Tartaglia, L., Sand, D., Wyatt, S., et al. 2017b, The Astronomer's Telegram, 10260
- . 2017c, The Astronomer's Telegram, 10439
- . 2017d, The Astronomer's Telegram, 10629
- . 2017e, The Astronomer's Telegram, 10637
- . 2017f, The Astronomer's Telegram, 10638
- . 2017g, The Astronomer's Telegram, 10158
- . 2017h, The Astronomer's Telegram, 10214
- Tartaglia, L., Fraser, M., Sand, D. J., et al. 2017i, ApJL, 836, L12
- Tonry, J., Denneau, L., Stalder, B., et al. 2016, The Astronomer's Telegram, 9749
- Tonry, J. L. 2011, PASP, 123, 58
- Tully, R. B., Courtois, H. M., Dolphin, A. E., et al. 2013, AJ, 146, 86
- Vacca, W. D., Cushing, M. C., & Rayner, J. T. 2003, PASP, 115, 389
- Valenti, S., Tartaglia, L., Sand, D., et al. 2017a, The Astronomer's Telegram, 10706
- Valenti, S., Sand, D., Pastorello, A., et al. 2014, MNRAS, 438, L101
- Valenti, S., Sand, D., Stritzinger, M., et al. 2015, MNRAS, 448, 2608
- Valenti, S., Howell, D. A., Stritzinger, M. D., et al. 2016, MNRAS, 459, 3939
- Valenti, S., David, Sand, J., et al. 2017b, ApJL, 848, L24
- Van Der Walt, S., Colbert, S. C., & Varoquaux, G. 2011, ArXiv e-prints, arXiv:1102.1523
- Van Dyk, S. D., Davidge, T. J., Elias-Rosa, N., et al. 2012a, AJ, 143, 19
- Van Dyk, S. D., Cenko, S. B., Poznanski, D., et al. 2012b, ApJ, 756, 131
- Vernet, J., Dekker, H., D'Odorico, S., et al. 2011, A&A, 536, A105
- White, D. J., Daw, E. J., & Dhillon, V. S. 2011, Classical and Quantum Gravity, 28, 085016
- Yaron, O., & Gal-Yam, A. 2012, PASP, 124, 668
- Yaron, O., Perley, D. A., Gal-Yam, A., et al. 2017, Nature Physics, 13, 510
- Zheng, W., Silverman, J. M., Filippenko, A. V., et al. 2013, ApJL, 778, L15

APPENDIX
A. PHOTOMETRIC TABLES

Table 2. *BV* and unfiltered light curves of DLT16am

Date	JD	phase d	<i>B</i> (err) (mag)	<i>V</i> (err) (mag)	<i>Open</i> (err) (mag)	Inst
20161117	2457709.590	-3.01	> 19.8	> 20.6	...	IO:O
20161117	2457710.070	-2.53	> 20.2	> 19.9	...	1m0-03
20161118	2457710.679	-1.92	> 20.5	PROMPT5
20161118	2457710.780	-1.82	...	> 21.0	...	EFOSC2
20161118	2457711.285	-1.31	> 20.8	> 20.5	...	1m0-10
20161119	2457711.510	-1.09	> 20.5	> 20.9	...	IO:O
20161119	2457711.687	-0.91	> 20.7	PROMPT5
20161119	2457711.760	-0.84	...	> 18.9	...	EFOSC2
20161119	2457712.325	-0.27	> 20.5	> 20.0	...	1m0-13
20161120	2457712.515	-0.08	> 20.0	IO:O
20161120	2457712.600	0.00	...	> 20.2	...	EFOSC
20161121	2457713.530	0.93	> 20.2	IO:O
20161121	2457713.600	1.00	...	20.84(0.52)	...	EFOSC
20161121	2457713.686	1.09	20.07(0.19)	PROMPT5
20161121	2457714.220	1.62	> 19.9	> 19.5	...	1m0-03
20161122	2457714.590	1.99	...	19.72(0.10)	...	EFOSC2
20161122	2457714.675	2.07	18.57(0.06)	PROMPT5
20161122	2457715.210	2.61	...	19.34(0.13)	...	1m0-11
20161122	2457715.210	2.61	> 20.5	1m0-11
20161123	2457715.540	2.94	18.27(0.05)	PROMPT5
20161123	2457716.045	3.44	...	19.18(0.15)	...	1m0-11
20161123	2457716.045	3.44	> 19.9	1m0-11
20161124	2457717.015	4.42	...	19.24(0.13)	...	1m0-03
20161124	2457717.015	4.42	> 20.4	1m0-03
20161125	2457717.530	4.93	> 20.7	1m0-05
20161125	2457717.542	4.94	18.14(0.05)	PROMPT5
20161125	2457718.110	5.51	> 19.7	1m0-03
20161125	2457718.420	5.82	> 21.0	1m0-10
20161126	2457718.562	5.96	18.02(0.05)	PROMPT5
20161126	2457718.760	6.16	...	19.27(0.22)	...	EFOSC2
20161126	2457718.825	6.23	...	19.21(0.11)	...	1m0-04

Table 2 continued

Table 2 (*continued*)

Date	JD	phase	$B(\text{err})$	$V(\text{err})$	$Open(\text{err})$	Inst
		d	(mag)	(mag)	(mag)	
20161126	2457718.825	6.23	> 20.2	1m0-04
20161127	2457719.543	6.94	18.00(0.05)	PROMPT5
20161127	2457720.290	7.69	...	19.18(0.10)	...	1m0-10
20161127	2457720.290	7.69	> 20.7	1m0-10
20161128	2457720.544	7.94	17.91(0.05)	PROMPT5
20161128	2457721.325	8.73	...	19.19(0.11)	...	1m0-13
20161128	2457721.325	8.73	> 20.7	1m0-13
20161129	2457721.535	8.94	> 20.0	IO:O
20161129	2457721.545	8.94	17.68(0.05)	PROMPT5
20161130	2457722.546	9.95	17.69(0.05)	PROMPT5
20161130	2457722.565	9.96	...	19.08(0.09)	...	1m0-10
20161130	2457722.565	9.96	> 21.1	1m0-10
20161130	2457723.415	10.81	...	19.23(0.10)	...	1m0-10
20161130	2457723.415	10.81	> 21.0	1m0-10
20161201	2457723.546	10.95	17.92(0.04)	PROMPT5
20161201	2457724.415	11.81	...	19.20(0.12)	...	1m0-12
20161201	2457724.415	11.81	> 20.7	1m0-12
20161202	2457724.546	11.95	17.89(0.04)	PROMPT5
20161202	2457725.310	12.71	> 21.7	1m0-10
20161202	2457725.310	12.71	...	19.25(0.10)	...	1m0-10
20161203	2457725.547	12.95	18.01(0.04)	PROMPT5
20161204	2457726.548	13.95	18.00(0.04)	PROMPT5
20161204	2457727.200	14.60	> 18.1	> 19.0	...	1m0-11
20161205	2457728.470	15.87	...	19.38(0.14)	...	IO:O
20161205	2457728.470	15.87	> 19.9	IO:O
20161205	2457727.549	14.95	17.90(0.07)	PROMPT5
20161206	2457728.549	15.95	17.99(0.05)	PROMPT5
20161206	2457728.620	16.02	18.02(0.04)	PROMPT5
20161207	2457729.550	16.95	18.10(0.04)	PROMPT5
20161207	2457729.623	17.02	18.03(0.04)	PROMPT5
20161207	2457730.130	17.53	...	19.42(0.13)	...	1m0-03
20161207	2457730.130	17.53	> 20.8	1m0-03
20161207	2457730.475	17.88	> 20.0	19.36(0.13)	...	IO:O
20161208	2457730.619	18.02	17.46(0.04)	PROMPT5
20161209	2457732.005	19.40	...	19.49(0.12)	...	1m0-03
20161209	2457732.005	19.40	> 20.6	1m0-03

Table 2 continued

Table 2 (*continued*)

Date	JD	phase	$B(\text{err})$	$V(\text{err})$	$Open(\text{err})$	Inst
		d	(mag)	(mag)	(mag)	
20161210	2457732.530	19.93	> 20.2	19.42(0.12)	...	IO:O
20161210	2457732.748	20.15	18.27(0.06)	PROMPT5
20161210	2457733.130	20.53	> 20.3	1m0-03
20161210	2457733.370	20.77	> 20.0	1m0-10
20161211	2457733.828	21.23	18.12(0.04)	PROMPT5
20161211	2457734.445	21.84	...	19.44(0.14)	...	IO:O
20161211	2457734.445	21.84	> 19.8	IO:O
20161212	2457734.553	21.95	18.22(0.05)	PROMPT5
20161213	2457735.500	22.90	> 19.8	IO:O
20161213	2457735.660	23.06	...	> 18.8	...	1m0-05
20161214	2457737.485	24.88	> 19.3	> 19.2	...	1m0-10
20161215	2457738.480	25.88	...	19.54(0.13)	...	1m0-10
20161216	2457738.625	26.02	18.18(0.04)	PROMPT5
20161217	2457739.556	26.96	18.15(0.04)	PROMPT5
20161218	2457740.556	27.96	18.19(0.03)	PROMPT5
20161218	2457740.730	28.13	...	19.50(0.06)	...	EFOSC2
20161219	2457741.556	28.96	18.17(0.04)	PROMPT5
20161220	2457742.500	29.90	...	19.58(0.13)	...	1m0-13
20161220	2457742.556	29.96	18.24(0.04)	PROMPT5
20161220	2457743.450	30.85	...	19.65(0.13)	...	1m0-13
20161221	2457744.370	31.77	...	19.69(0.15)	...	1m0-13
20161222	2457744.557	31.96	18.22(0.04)	PROMPT5
20161223	2457745.686	33.09	18.18(0.04)	PROMPT5
20161224	2457746.557	33.96	18.27(0.04)	PROMPT5
20161225	2457747.575	34.98	18.22(0.04)	PROMPT5
20161225	2457748.470	35.87	...	> 19.5	...	1m0-10
20161226	2457749.450	36.85	...	19.61(0.13)	...	1m0-13
20161227	2457749.558	36.96	18.33(0.05)	PROMPT5
20161227	2457750.350	37.75	...	19.75(0.12)	...	1m0-12
20161228	2457750.558	37.96	18.30(0.04)	PROMPT5
20161228	2457751.450	38.85	...	19.57(0.16)	...	1m0-13
20161229	2457751.559	38.96	18.40(0.04)	PROMPT5
20161229	2457752.350	39.75	...	19.77(0.12)	...	1m0-13
20161230	2457752.559	39.96	18.33(0.04)	PROMPT5
20161230	2457753.495	40.90	...	19.75(0.13)	...	1m0-12
20161230	2457753.495	40.90	> 20.8	1m0-12

Table 2 continued

Table 2 (*continued*)

Date	JD	phase	$B(\text{err})$	$V(\text{err})$	$Open(\text{err})$	Inst
		d	(mag)	(mag)	(mag)	
20161231	2457753.559	40.96	18.28(0.04)	PROMPT5
20170101	2457754.559	41.96	18.35(0.04)	PROMPT5
20170102	2457755.559	42.96	18.44(0.05)	PROMPT5
20170102	2457755.740	43.14	> 21.1	1m0-04
20170103	2457756.562	43.96	18.51(0.07)	PROMPT5
20170103	2457756.715	44.11	...	20.08(0.12)	...	1m0-05
20170103	2457756.715	44.11	> 21.1	1m0-05
20170106	2457759.559	46.96	18.46(0.06)	PROMPT5
20170106	2457759.720	47.12	...	19.75(0.06)	...	EFOSC2
20170107	2457760.559	47.96	18.42(0.08)	PROMPT5
20170111	2457764.595	52.00	...	19.93(0.15)	...	1m0-05
20170111	2457764.595	52.00	> 21.3	1m0-05
20170116	2457769.671	57.07	18.48(0.07)	PROMPT5
20170117	2457770.558	57.96	18.49(0.05)	PROMPT5
20170118	2457771.558	58.96	18.45(0.05)	PROMPT5
20170118	2457771.590	58.99	...	20.07(0.49)	...	EFOSC2
20170119	2457772.557	59.96	18.53(0.06)	PROMPT5
20170119	2457772.635	60.03	...	20.04(0.14)	...	1m0-05
20170119	2457772.635	60.03	> 21.1	1m0-05
20170120	2457773.557	60.96	18.49(0.05)	PROMPT5
20170120	2457773.695	61.09	...	20.21(0.15)	...	1m0-05
20170120	2457773.695	61.09	> 22.4	1m0-05
20170121	2457774.685	62.08	...	20.06(0.14)	...	1m0-04
20170121	2457774.685	62.08	> 20.9	1m0-04
20170124	2457777.699	65.10	18.28(0.08)	PROMPT5
20170125	2457778.613	66.01	18.71(0.07)	PROMPT5
20170125	2457778.613	66.01	19.15(0.08)	PROMPT5
20170126	2457779.620	67.02	...	20.22(0.33)	...	EFOSC2
20170127	2457781.280	68.68	...	20.03(0.18)	...	1m0-13
20170128	2457781.559	68.96	18.57(0.07)	PROMPT5
20170129	2457782.554	69.95	18.48(0.06)	PROMPT5
20170130	2457783.551	70.95	18.58(0.06)	PROMPT5
20170131	2457784.554	71.95	18.67(0.07)	PROMPT5
20170131	2457785.290	72.69	...	20.19(0.16)	...	1m0-13
20170201	2457785.553	72.95	18.73(0.07)	PROMPT5
20170202	2457786.549	73.95	18.65(0.06)	PROMPT5

Table 2 continued

Table 2 (*continued*)

Date	JD	phase	$B(\text{err})$	$V(\text{err})$	$Open(\text{err})$	Inst
		d	(mag)	(mag)	(mag)	
20170203	2457787.550	74.95	18.60(0.07)	PROMPT5
20170204	2457789.300	76.70	...	20.16(0.16)	...	1m0-13
20170205	2457789.580	76.98	...	20.36(0.34)	...	EFOSC2
20170205	2457789.590	76.99	...	20.14(0.20)	...	1m0-04
20170208	2457793.340	80.74	...	> 19.9	...	1m0-13
20170209	2457793.576	80.98	18.81(0.07)	PROMPT5
20170211	2457795.550	82.95	18.82(0.06)	PROMPT5
20170212	2457796.542	83.94	19.06(0.09)	PROMPT5
20170213	2457797.541	84.94	19.12(0.11)	PROMPT5
20170213	2457797.920	85.32	...	20.58(0.18)	...	1m0-03
20170213	2457798.380	85.78	...	> 20.0	...	1m0-10
20170214	2457798.541	85.94	19.17(0.08)	PROMPT5
20170214	2457799.360	86.76	...	> 20.0	...	1m0-13
20170215	2457799.540	86.94	19.54(0.11)	PROMPT5
20170218	2457803.260	90.66	...	> 20.4	...	1m0-13
20170218	2457802.530	89.93	...	> 21.4	...	EFOSC2
20170219	2457803.550	90.95	...	> 21.1	...	EFOSC2
20170219	2457803.930	91.33	...	> 20.6	...	1m0-03
20170221	2457805.610	93.01	...	> 20.5	...	1m0-05
20170222	2457806.930	94.33	...	> 20.6	...	1m0-03
20170223	2457807.940	95.34	...	> 20.7	...	1m0-11
20170224	2457808.980	96.38	...	> 20.4	...	1m0-11
20170225	2457810.300	97.70	...	> 20.5	...	1m0-13
20170225	2457809.530	96.93	...	20.99(0.56)	...	EFOSC
20170226	2457810.900	98.30	...	> 20.5	...	1m0-03
20170301	2457814.300	101.70	...	> 20.9	...	1m0-13
20170302	2457815.300	102.70	...	> 20.5	...	1m0-10
20170303	2457816.290	103.69	...	> 20.6	...	1m0-12
20170306	2457818.500	105.90	...	> 21.0	...	EFOSC
20170308	2457820.500	107.90	...	21.14(0.06)	...	EFOSC
20170312	2457824.920	112.32	...	> 19.8	...	2m0-02

NOTE— PROMPT5: 0.41m PROMPT5 telescope at the Cerro Tololo Inter-American Observatory, Chile; EFOSC2: 3.58 m ESO New Technology Telescope with EFOSC2 at the ESO La Silla Observatory, Chile; IO:O: 2 m 2 m Liverpool Telescope with IO:O, at the Observatorio del Roque de Los Muchachos, Spain; Las Cumbres Observatory 1m0-03, 1m0-11: node at Siding Spring, Australia; 1m0-04, 1m0-05, 2m0-02: node at Cerro Tololo Inter-American Observatory, Chile; 1m0-10, 1m0-12, 1m0-13: node at South African Astronomical Observatory, South Africa.

Table 3. *griz* light curves of DLT16am

Date	JD	phase	<i>g</i> (err)	<i>r</i> (err)	<i>i</i> (err)	<i>z</i> (err)	Inst
		d	(mag)	(mag)	(mag)	(mag)	
20161116	2457708.60	-4.00	> 18.7	> 18.0	IO:O
20161117	2457709.53	-3.07	...	> 20.4	> 19.9	> 19.8	GROND
20161117	2457709.60	-3.00	> 19.3	> 18.4	IO:O
20161118	2457710.53	-2.08	> 19.3	> 18.8	IO:O
20161118	2457711.29	-1.31	> 21.7	1m0-10
20161118	2457711.30	-1.31	...	> 21.0	> 20.2	...	1m0-10
20161119	2457711.52	-1.08	> 19.4	> 18.7	IO:O
20161119	2457711.78	-0.82	> 21.8	> 17.1	GROND
20161119	2457712.34	-0.27	...	> 20.5	> 19.6	...	1m0-13
20161120	2457712.52	-0.08	> 19.0	> 18.6	IO:O
20161121	2457713.53	0.92	...	20.37(0.45)	PROMPT1
20161121	2457713.54	0.94	> 18.9	> 18.4	IO:O
20161121	2457713.61	1.01	...	20.18(0.23)	PROMPT1
20161121	2457713.69	1.09	...	20.02(0.15)	PROMPT1
20161121	2457713.81	1.21	...	19.88(0.22)	18.95(0.16)	...	E2V
20161121	2457714.23	1.63	> 20.8	1m0-03
20161121	2457714.24	1.63	...	19.28(0.19)	18.34(0.21)	...	1m0-03
20161122	2457714.55	1.94	20.87(0.28)	...	17.94(0.17)	17.17(0.10)	IO:O
20161122	2457714.55	1.94	...	18.90(0.12)	PROMPT1
20161122	2457714.63	2.03	...	18.89(0.10)	PROMPT1
20161122	2457714.67	2.07	20.83(0.17)	18.81(0.08)	17.91(0.04)	17.06(0.05)	GROND
20161122	2457714.71	2.11	...	18.88(0.17)	PROMPT1
20161122	2457714.80	2.20	...	18.83(0.11)	PROMPT1
20161122	2457715.23	2.63	...	18.74(0.11)	17.74(0.09)	...	1m0-11
20161123	2457715.63	3.03	...	18.76(0.11)	17.60(0.08)	...	E2V
20161123	2457715.73	3.13	...	18.73(0.12)	PROMPT1
20161123	2457716.05	3.45	20.46(0.16)	1m0-11
20161123	2457716.06	3.46	...	18.46(0.07)	17.51(0.08)	...	1m0-11
20161124	2457716.55	3.95	...	18.66(0.10)	PROMPT1
20161124	2457716.60	4.00	...	18.69(0.25)	E2V
20161124	2457716.68	4.08	20.65(0.10)	18.61(0.07)	17.27(0.05)	...	GROND
20161124	2457717.02	4.42	20.47(0.14)	1m0-03
20161124	2457717.03	4.42	...	18.60(0.04)	17.51(0.06)	...	1m0-03
20161125	2457717.54	4.94	20.52(0.14)	1m0-05
20161125	2457717.55	4.95	...	18.50(0.08)	17.44(0.04)	...	1m0-05
20161125	2457717.69	5.09	20.44(0.04)	18.61(0.07)	17.43(0.03)	16.53(0.04)	GROND

Table 3 continued

Table 3 (*continued*)

Date	JD	phase	$g(\text{err})$	$r(\text{err})$	$i(\text{err})$	$z(\text{err})$	Inst
		d	(mag)	(mag)	(mag)	(mag)	
20161125	2457717.76	5.16	...	18.54(0.11)	PROMPT1
20161125	2457717.77	5.17	...	18.60(0.08)	17.42(0.05)	...	E2V
20161125	2457718.12	5.52	20.11(0.23)	1m0-03
20161125	2457718.12	5.52	...	18.48(0.08)	17.43(0.06)	...	1m0-03
20161125	2457718.44	5.84	20.55(0.13)	1m0-10
20161125	2457718.45	5.85	...	18.47(0.06)	17.38(0.03)	...	1m0-10
20161126	2457718.84	6.24	20.40(0.13)	1m0-04
20161126	2457718.85	6.25	...	18.51(0.07)	17.33(0.06)	...	1m0-04
20161127	2457719.84	7.24	...	18.52(0.12)	PROMPT1
20161127	2457720.31	7.71	...	18.51(0.06)	17.31(0.04)	...	1m0-10
20161128	2457720.81	8.21	...	18.61(0.10)	17.37(0.10)	...	E2V
20161128	2457721.34	8.74	20.58(0.12)	1m0-13
20161128	2457721.35	8.75	...	18.47(0.12)	17.27(0.05)	...	1m0-13
20161129	2457721.54	8.94	20.39(0.17)	18.35(0.09)	17.23(0.03)	16.35(0.03)	IO:O
20161129	2457721.62	9.02	20.55(0.08)	18.45(0.05)	17.24(0.01)	16.32(0.02)	GROND
20161129	2457721.72	9.11	...	18.60(0.15)	17.33(0.14)	...	E2V
20161130	2457722.58	9.98	20.49(0.13)	1m0-10
20161130	2457722.59	9.98	...	18.40(0.07)	17.24(0.03)	...	1m0-10
20161130	2457722.71	10.11	17.16(0.20)	...	E2V
20161130	2457723.43	10.83	20.49(0.10)	1m0-10
20161130	2457723.44	10.83	...	18.45(0.07)	17.24(0.03)	...	1m0-10
20161130	2457723.50	10.90	16.28(0.11)	IO:O
20161201	2457723.53	10.93	...	18.47(0.10)	PROMPT1
20161201	2457723.81	11.21	...	18.45(0.10)	PROMPT1
20161201	2457724.43	11.82	20.68(0.13)	1m0-12
20161201	2457724.44	11.83	...	18.45(0.05)	17.22(0.03)	...	1m0-12
20161202	2457724.54	11.94	...	18.48(0.10)	PROMPT1
20161202	2457724.76	12.16	...	18.50(0.10)	PROMPT1
20161202	2457724.84	12.24	...	18.43(0.08)	PROMPT1
20161202	2457725.32	12.72	20.45(0.12)	1m0-10
20161202	2457725.33	12.73	...	18.48(0.06)	17.25(0.03)	16.43(0.05)	1m0-10
20161204	2457726.73	14.13	...	18.25(0.17)	17.49(0.16)	...	E2V
20161204	2457727.21	14.61	20.40(0.24)	1m0-11
20161205	2457728.48	15.88	20.55(0.19)	18.49(0.06)	17.29(0.03)	16.39(0.03)	IO:O
20161206	2457728.53	15.93	...	18.55(0.10)	PROMPT1
20161206	2457728.74	16.14	...	18.31(0.27)	E2V

Table 3 continued

Table 3 (*continued*)

Date	JD	phase	$g(\text{err})$	$r(\text{err})$	$i(\text{err})$	$z(\text{err})$	Inst
		d	(mag)	(mag)	(mag)	(mag)	
20161207	2457730.15	17.54	20.74(0.15)	1m0-03
20161207	2457730.15	17.55	...	18.62(0.11)	17.41(0.05)	16.62(0.09)	1m0-03
20161207	2457730.48	17.88	> 19.8	IO:O
20161207	2457730.48	17.88	...	18.54(0.13)	17.35(0.05)	...	IO:O
20161209	2457732.02	19.42	20.60(0.20)	1m0-03
20161209	2457732.03	19.43	...	18.58(0.09)	17.47(0.04)	16.77(0.05)	1m0-03
20161210	2457732.54	19.94	20.60(0.19)	18.61(0.15)	17.40(0.05)	16.44(0.03)	IO:O
20161210	2457733.15	20.55	20.65(0.25)	1m0-03
20161210	2457733.16	20.55	...	18.56(0.17)	17.51(0.09)	16.63(0.08)	1m0-03
20161210	2457733.41	20.80	...	18.70(0.14)	17.56(0.09)	16.63(0.11)	1m0-10
20161210	2457733.45	20.85	17.45(0.14)	16.46(0.13)	IO:O
20161211	2457734.45	21.84	20.63(0.17)	18.64(0.12)	17.49(0.07)	16.49(0.03)	IO:O
20161213	2457735.51	22.90	> 19.7	IO:O
20161213	2457735.51	22.90	17.50(0.08)	16.50(0.08)	IO:O
20161213	2457735.67	23.07	20.60(0.25)	1m0-09
20161213	2457736.47	23.86	...	18.55(0.10)	17.48(0.04)	16.50(0.03)	IO:O
20161213	2457736.50	23.90	...	18.73(0.14)	17.66(0.04)	16.60(0.08)	ALFOSC_FASU
20161213	2457736.50	23.90	> 19.8	ALFOSC_FASU
20161214	2457737.47	24.86	17.55(0.12)	...	IO:O
20161215	2457737.50	24.90	20.61(0.41)	1m0-10
20161215	2457737.51	24.91	...	18.85(0.10)	17.60(0.10)	16.70(0.09)	1m0-10
20161215	2457738.50	25.90	20.99(0.22)	1m0-10
20161215	2457738.50	25.90	...	18.58(0.09)	17.52(0.06)	16.70(0.07)	1m0-10
20161220	2457743.46	30.86	21.30(0.18)	1m0-13
20161220	2457743.47	30.87	...	18.72(0.10)	17.58(0.04)	16.74(0.05)	1m0-13
20161220	2457742.73	30.13	17.54(0.07)	...	EFOSC
20161221	2457744.38	31.78	21.15(0.18)	1m0-13
20161221	2457744.39	31.79	...	18.70(0.06)	17.57(0.03)	16.71(0.04)	1m0-13
20161223	2457745.72	33.11	...	18.58(0.30)	E2V
20161225	2457748.48	35.88	21.28(0.30)	1m0-10
20161225	2457748.49	35.88	...	18.93(0.20)	17.69(0.12)	16.66(0.11)	1m0-10
20161226	2457749.46	36.86	21.02(0.17)	1m0-13
20161226	2457749.47	36.87	...	18.71(0.13)	17.63(0.05)	16.70(0.06)	1m0-13
20161227	2457750.36	37.76	> 20.8	1m0-12
20161228	2457751.46	38.86	21.40(0.36)	1m0-13
20161228	2457751.47	38.87	...	18.57(0.14)	17.64(0.08)	16.73(0.10)	1m0-13

Table 3 continued

Table 3 (*continued*)

Date	JD	phase	$g(\text{err})$	$r(\text{err})$	$i(\text{err})$	$z(\text{err})$	Inst
		d	(mag)	(mag)	(mag)	(mag)	
20161229	2457752.36	39.76	21.52(0.18)	1m0-13
20161229	2457752.37	39.77	...	18.76(0.07)	17.64(0.03)	16.72(0.04)	1m0-13
20161230	2457752.74	40.13	...	18.75(0.20)	E2V
20161231	2457753.51	40.91	21.04(0.20)	1m0-12
20161231	2457753.52	40.92	...	18.75(0.10)	17.70(0.06)	...	1m0-12
20170103	2457756.73	44.13	> 21.1	1m0-09
20170103	2457756.74	44.13	...	18.76(0.06)	17.63(0.08)	...	1m0-05
20170104	2457758.40	45.80	17.67(0.11)	...	IO:O
20170111	2457764.62	52.02	...	18.78(0.06)	17.70(0.04)	...	1m0-05
20170115	2457769.35	56.75	...	18.81(0.12)	17.66(0.05)	...	IO:O
20170116	2457770.41	57.80	...	18.87(0.05)	17.75(0.01)	16.71(0.01)	ALFOSC_FASU
20170116	2457770.41	57.80	> 20.4	ALFOSC_FASU
20170119	2457772.66	60.05	...	18.82(0.08)	17.76(0.03)	...	1m0-05
20170120	2457773.71	61.11	> 21.0	1m0-09
20170120	2457773.72	61.11	...	18.87(0.09)	17.73(0.05)	...	1m0-05
20170121	2457774.70	62.10	21.55(0.28)	1m0-04
20170121	2457774.71	62.10	...	18.93(0.09)	17.76(0.04)	...	1m0-04
20170122	2457775.68	63.07	...	18.82(0.34)	E2V
20170122	2457776.03	63.43	21.50(0.22)	1m0-11
20170122	2457776.04	63.44	...	18.95(0.09)	17.80(0.05)	16.81(0.06)	1m0-11
20170122	2457776.43	63.83	21.20(0.14)	1m0-10
20170122	2457776.45	63.84	...	18.84(0.08)	17.75(0.04)	16.86(0.06)	1m0-10
20170124	2457778.37	65.77	> 20.4	> 17.6	IO:O
20170126	2457779.62	67.02	...	18.92(0.08)	E2V
20170126	2457780.34	67.73	> 20.9	IO:O
20170126	2457780.34	67.73	...	18.92(0.14)	17.73(0.05)	...	IO:O
20170127	2457780.65	68.04	...	18.96(0.08)	E2V
20170127	2457781.29	68.69	21.45(0.24)	1m0-13
20170127	2457781.30	68.70	...	18.92(0.15)	17.92(0.06)	16.87(0.07)	1m0-13
20170128	2457782.34	69.74	> 20.6	IO:O
20170128	2457782.34	69.74	...	18.95(0.16)	17.90(0.05)	...	IO:O
20170131	2457785.31	72.71	21.69(0.20)	1m0-13
20170131	2457785.32	72.71	...	19.07(0.08)	17.94(0.04)	16.93(0.03)	1m0-13
20170202	2457787.38	74.78	> 20.7	IO:O
20170202	2457787.38	74.78	...	19.04(0.10)	17.96(0.06)	...	IO:O
20170204	2457789.31	76.71	22.05(0.47)	1m0-13

Table 3 continued

Table 3 (*continued*)

Date	JD	phase d	$g(\text{err})$ (mag)	$r(\text{err})$ (mag)	$i(\text{err})$ (mag)	$z(\text{err})$ (mag)	Inst
20170204	2457789.33	76.73	...	19.17(0.16)	18.07(0.06)	17.02(0.06)	1m0-13
20170205	2457789.60	77.00	22.01(0.29)	1m0-04
20170205	2457789.62	77.02	...	19.05(0.12)	17.97(0.05)	16.97(0.07)	1m0-04
20170207	2457792.39	79.79	> 20.4	> 16.4	IO:O
20170207	2457792.39	79.79	...	19.44(0.10)	18.20(0.06)	...	IO:O
20170208	2457792.66	80.05	...	18.92(0.32)	18.07(0.10)	...	E2V
20170208	2457793.36	80.76	...	19.25(0.13)	18.13(0.13)	17.14(0.09)	1m0-13
20170213	2457797.94	85.34	> 21.4	1m0-03
20170213	2457797.95	85.35	...	19.56(0.18)	18.53(0.13)	17.33(0.15)	1m0-03
20170213	2457798.35	85.75	> 21.2	1m0-13
20170213	2457798.36	85.75	...	19.62(0.10)	18.52(0.10)	...	1m0-13
20170214	2457799.38	86.78	> 21.5	1m0-12
20170214	2457799.39	86.79	...	20.00(0.14)	18.76(0.14)	...	1m0-12
20170216	2457801.28	88.67	...	19.92(0.16)	18.91(0.07)	...	1m0-13
20170218	2457802.63	90.02	...	20.33(0.37)	E2V
20170218	2457803.29	90.69	...	20.24(0.11)	19.22(0.14)	...	1m0-13
20170219	2457803.57	90.97	> 21.6	1m0-05
20170220	2457804.57	91.97	> 22.7	1m0-09
20170220	2457804.59	91.98	...	20.29(0.14)	19.26(0.11)	...	1m0-05
20170220	2457804.63	92.03	...	20.37(0.29)	19.18(0.16)	...	E2V
20170221	2457805.92	93.32	> 21.8	1m0-03
20170221	2457805.94	93.33	...	20.50(0.08)	19.48(0.11)	...	1m0-03
20170222	2457806.59	93.98	...	> 19.1	> 18.7	...	1m0-08
20170223	2457807.63	95.02	...	20.67(0.08)	19.51(0.10)	...	1m0-05
20170224	2457809.31	96.71	> 21.9	1m0-10
20170224	2457809.32	96.71	...	20.73(0.15)	19.55(0.19)	...	1m0-10
20170225	2457810.31	97.71	> 21.6	1m0-13
20170225	2457810.32	97.72	...	20.69(0.10)	1m0-13
20170225	2457810.32	97.72	> 19.5	...	1m0-13
20170226	2457810.91	98.31	> 21.9	1m0-11
20170226	2457810.93	98.32	...	20.74(0.10)	19.59(0.15)	...	1m0-11
20170301	2457814.33	101.73	...	20.75(0.16)	19.69(0.16)	18.20(0.15)	1m0-13
20170302	2457815.32	102.72	...	20.74(0.09)	19.71(0.11)	18.20(0.12)	1m0-10
20170303	2457816.31	103.71	...	20.81(0.10)	19.74(0.13)	18.19(0.10)	1m0-12
20170305	2457817.56	104.96	...	20.83(0.55)	E2V
20170306	2457818.56	105.96	...	20.92(0.08)	19.74(0.14)	18.28(0.16)	1m0-05

Table 3 continued

Table 3 (*continued*)

Date	JD	phase	$g(\text{err})$	$r(\text{err})$	$i(\text{err})$	$z(\text{err})$	Inst
		d	(mag)	(mag)	(mag)	(mag)	
20170310	2457822.50	109.90	...	20.91(0.09)	E2V
20170315	2457827.56	114.96	...	> 19.54	E2V
20170316	2457828.54	115.94	...	> 19.79	E2V

NOTE— IO:O: 2 m Liverpool Telescope with IO:O; GROND: MPG/ESO 2.2 m telescope with GROND at the ESO La Silla Observatory, Chile; PROMPT1: 0.41 m PROMPT1 telescope at the Cerro Tololo Inter-American Observatory, Chile; ALFOSC_FASU: 2.56 m Nordic Optical Telescope with ALFOSC_FASU, at the Observatorio del Roque de los Muchachos, Spain; E2V: Las Campanas Observatory 1 m Swope Telescope with the E2V camera, at the Las Campanas Observatory, Chile; Las Cumbres Observatory 1m0-03, 1m0-11: node at Siding Spring, Australia; 1m0-04, 1m0-05, 1m0-09: node at Cerro Tololo Inter-American Observatory, Chile; 1m0-10, 1m0-12, 1m0-13: node at South African Astronomical Observatory, South Africa.

Table 4. NIR light curves of DLT16am

JD	phase	$J(\text{err})$ (mag)	$H(\text{err})$ (mag)	$K(\text{err})$ (mag)	Inst
2457707.77	-4.83	> 18.3	> 17.7	> 16.4	GROND
2457708.73	-3.87	> 19.0	> 18.2	> 16.7	GROND
2457709.53	-3.07	> 18.4	> 17.3	> 16.1	GROND
2457711.78	-0.82	...	> 15.9	...	GROND
2457714.67	2.07	15.10(0.29)	14.69(0.19)	14.05(0.19)	GROND
2457716.68	4.08	15.03(0.21)	14.29(0.19)	13.75(0.25)	GROND
2457717.69	5.09	14.70(0.15)	14.11(0.22)	13.39(0.23)	GROND
2457721.62	9.02	14.49(0.24)	13.80(0.30)	13.31(0.22)	GROND
2457763.39	50.79	14.56(0.18)	13.79(0.13)	13.28(0.31)	NOTCam
2457772.74	60.14	14.65(0.18)	13.85(0.31)	13.26(0.31)	SOFI
2457790.68	78.07	14.85(0.21)	13.90(0.32)	13.47(0.21)	SOFI
2457791.38	78.78	14.81(0.22)	14.01(0.24)	13.49(0.32)	NOTCam
2457804.52	91.92	16.04(0.17)	15.72(0.21)	15.16(0.31)	SOFI
2457819.52	106.92	16.40(0.15)	15.61(0.27)	14.79(0.30)	SOFI

NOTE—GROND: MPG/ESO 2.2 m telescope with GROND, at the ESO La Silla Observatory, Chile. NOTCam: 2.56m Nordic Optical Telescope with NOTCam, at the Observatorio del Roque de los Muchachos, La Palma, Spain; SOFI: 3.58 m ESO New Technology Telescope with SOFI, at the ESO La Silla Observatory, Chile.